

Chlorine oxidation of VOCs at a semi-rural site in Beijing: Significant chlorine liberation from ClNO₂ and subsequent gas and particle phase Cl-VOC production

Michael Le Breton¹, Åsa M Hallquist², Ravi Kant Pathak¹, David Simpson^{3,4}, Yujue Wang⁵, John Johansson³, Jing Zheng⁵, Yudong Yang⁵, Dongjie Shang⁵, Haichao Wang⁵, Qianyun Liu⁶, Chak Chan⁷, Tao Wang⁸, Thomas J. Bannan⁹, Michael Priestley⁹, Carl J. Percival^{9*}, Dudley E. Shallcross^{10,11}, Keding Lu⁵, Song Guo⁵, Min Hu⁵ and Mattias Hallquist¹

¹Department of Chemistry and Molecular Biology, University of Gothenburg, Gothenburg, Sweden

²IVL Swedish Environmental Research Institute, Gothenburg, Sweden

³Earth and Space Sciences, Chalmers University of Technology, Gothenburg, Sweden

⁴Norwegian Meteorological Institute, Oslo, Norway

⁵State Key Joint Laboratory of Environmental Simulation and Pollution Control, College of Environmental Sciences and Engineering, Peking University, Beijing, China

⁶Division of Environment and Sustainability, The Hong Kong University of Science and Technology, Clearwater Bay, Kowloon, Hong Kong

⁷School of Energy and Environment, City University of Hong Kong, Hong Kong

⁸Department of Civil and Environmental Engineering, The Hong Kong Polytechnic University, Hong Kong, China

⁹Centre for Atmospheric Science, School of Earth, Atmospheric and Environmental Science, University of Manchester, Manchester, UK

¹⁰School of Chemistry, University of Bristol, Cantock's Close, Bristol, BS8 1TS, UK

¹¹Department of Chemistry, University of the Western Cape, Bellville, Cape Town, South Africa.

* Now at Jet Propulsion Laboratory, California Institute of Technology, 4800 Oak Grove Drive, Pasadena, California, USA.

Correspondence to: M. le Breton (Michael.le.breton@gu.se)

Abstract. Nitryl Chloride (ClNO₂) accumulation at night-time acts as a significant reservoir for active chlorine and impacts the following day's photochemistry when the chlorine atom is liberated at sunrise. Here, we report simultaneous measurements of N₂O₅ and a suite of inorganic halogens including ClNO₂ and Cl-VOCs in the gas and particle phase utilizing the FIGAERO-ToF-CIMS during an intensive measurement campaign 40 km Northwest of Beijing in May and June 2016. A maximum mixing ratio of 2900 ppt of ClNO₂ was observed with a mean campaign night-time mixing ratio of 487 ppt, appearing to have an anthropogenic source supported by correlation with SO₂, CO and benzene, which often persisted at high levels after sunrise until midday. This was attributed to such high mixing ratios persisting after numerous e-folding times of the photolytic lifetime enabling the chlorine atom production to reach 2.3 x 10⁵ molecules cm⁻³ from ClNO₂ alone, peaking at 9:30 am and up to 8.4 x 10⁵ molecules cm⁻³ when including the supporting inorganic halogen measurements.

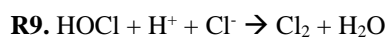
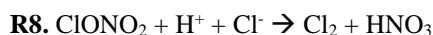
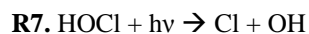
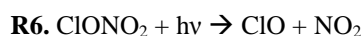
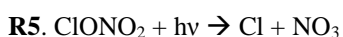
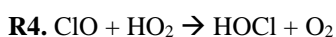
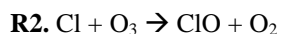
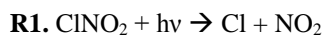
Cl-VOCs were observed in the particle and gas phase for the first time at high time resolution and illustrate how the iodide ToF-CIMS can detect unique markers of chlorine atom chemistry in ambient air from both biogenic and anthropogenic sources. Their presence and abundance can be explained via time series of their measured and steady state calculated precursors, enabling the assessment of competing OH and chlorine atom oxidation via measurements of products from both of these mechanisms and their relative contribution to SOA formation.

1
2
3
4
5
6
7
8
9
10
11
12
13
14
15
16
17
18
19
20
21
22
23
24
25
26
27
28
29
30
31

1. Introduction

NO and NO₂ (NO_x) are important catalysts in the photochemical production of ozone (O₃) playing a significant role in the oxidation of volatile organic compounds (VOCs) and subsequently have an adverse effect on air quality. In the daytime NO_x is primarily removed by the hydroxyl radical (OH) to form nitric acid (HNO₃), which is subsequently lost by wet deposition, becoming a major component of acid rain. At night-time, the OH radical is not a significant oxidant as photolysis stops, enabling the reaction between NO₂ and O₃ to form significant levels of the nitrate radical (NO₃) (Atkinson, 2000). NO₃ can accumulate at night or further react with NO₂ leading to the formation of N₂O₅ (Brown *et al.*, 2003b, Brown and Stutz, 2012). This equilibrium can lead to the reaction of NO₃ with VOCs at night forming organic nitrates or act as an important intermediate for heterogeneous reaction on aerosols as N₂O₅ produces NO₃⁻ and NO₂⁺ in the aqueous phase (Hallquist *et al.* 1999, Hallquist *et al.*, 2000, Wagner *et al.*, 2013). In the presence of chlorine, which is assumed in models to predominantly come from sea salt (Baker *et al.*, 2016), nitryl chloride (ClNO₂) can be formed and released into the gas phase from the aerosol surface (Osthoff *et al.*, 2008). ClNO₂ formation thereafter acts as a night-time radical reservoir due to its stability at night.

At sunrise ClNO₂ is rapidly photolysed, liberating the highly reactive chlorine atom subsequently converting it into ClO, HOCl and ClONO₂ depending on the available sunlight, O₃, HO_x and NO_x levels via the following reaction pathways (R1-R11).



The liberated chlorine will predominantly react with VOCs, with the pathways listed (R2-R11) representing alternative routes to loss of the chloride radical, and contribute to daytime photochemical oxidation, competing

1 with OH and perturbing standard organic peroxy radical abundance ($RO_x = OH + HO_2 + RO_2$), O_3 production rate,
2 NO_x lifetime and partitioning between reactive forms of nitrogen (Riedel et al., 2014). The rate constants for the
3 reaction of chlorine atoms with a number of VOCs is round 200 times larger than the equivalent reaction with OH
4 (Tanaka *et al.*, 2003); therefore, its abundance, fate and cycling can significantly alter standard daytime oxidation
5 pathways. The oxidation of VOCs by chlorine atoms is thought to be significant in the early hours of the day while
6 OH mixing ratios are low and chlorine atom production is high through the photolysis of $ClNO_2$, as well as feeding
7 into the standard HO_x/NO_x cycles via production of peroxy radicals from reactions with alkanes. Additional Cl_2
8 photolysis and HCl reaction with OH can also produce chlorine atoms throughout the day but at lower rates.

9 Saturated hydrocarbons are usually oxidised by reaction with OH or chlorine atom to form an organic peroxy
10 radical (RO_2), and H_2O or HCl depending on the oxidant (R12 and R13), which is the dominant pathway for
11 chloride-VOC reactions. In a heavily polluted environment such as Beijing, the RO_2 favours further reactions with
12 NO to form an oxygenated volatile organic compound, HO_2 and NO_2 or an alkyl nitrate $RONO_2$. Specifically, acyl
13 peroxy radicals can also react with NO_2 to form acyl peroxy nitrates (APN) such as peroxy acetyl nitrate (PAN).



19 Addition of the chlorine atom to unsaturated VOC can also occur and then continue on the similar reaction pathway
20 as denoted by R12 – R15. These pathways result in the production of unique chlorine atom chemistry markers
21 which have been previously investigated to indicate the extent of chlorine atom oxidation reactions (Riemer *et al.*,
22 2008, Keil and Shepson, 2006). The utilization of these compounds, such as 2-chloroperoxypropionyl nitrate (2-
23 Cl PPN) and 1-chloro-3-methyl-3butene-2-one (CMBO) as chlorine atom chemistry markers relies on the
24 abundance of the chlorine atom, the VOC precursor; HO_x , NO_x and O_3 and competing pathways for chlorine atom
25 reactions. Riedel *et al.* (2014) calculated that up to ten parts per trillion (ppt) Cl-VOCs are formed as a result of
26 chlorine atom addition to alkenes and can therefore provide a number of potential periods of dominating active Cl
27 chemistry (Wang *et al.*, 2001).

28 The production of chloroperoxy radicals via chlorine atom addition can lead to the formation of semi volatile
29 oxidation products which have been observed for both biogenic (Cai and Griffin *et al.*, 2006) and anthropogenic
30 emissions (Huang *et al.*, 2014, Riva *et al.*, 2015) in controlled laboratory studies. Chlorine initiated oxidation of
31 isoprene could also represent a significant oxidation pathway due to its rapid reaction rate compared with OH
32 (Orlando *et al.*, 2003) resulting in gas phase products such as chloroacetaldehyde and CMBO, a unique tracer for
33 atmospheric chlorine atom chemistry (Nordmeyer *et al.*, 1997). Furthermore, reactions of the chlorine atom with
34 isoprene or its SOA derived products could serve as an atmospheric chlorine sink (Ofner *et al.*, 2012). Wang *et al.*
35 (2017) revealed chlorine initiated oxidation of isoprene can produce SOA yields up to 36%, with products similar

1 to that of OH isoprene oxidation, compared with the 15% yield from standard oxidation calculated by Liu *et al.*
2 (2016), although this is known to be a factor of 2 higher than utilised in standard climate models. This SOA
3 formation from chlorine initiated oxidation presents a large knowledge gap in the literature, which to date is limited
4 by measurement capabilities.

5 This complex system results in a large uncertainty in the global budget of chlorine atoms $\sim 15\text{--}40 \text{ Tg Cl yr}^{-1}$
6 calculated by indirect means (Allan *et al.*, 2007; Platt *et al.*, 2004), which is further limited by the ability of
7 measurement techniques to accurately quantify short lived species at low mixing ratios. Our knowledge of the Cl
8 budget therefore depends on the accurate measurement of its precursors, namely ClNO₂ and major reaction
9 pathways of the chlorine atom upon liberation in the daytime. Measurements to date show that the mixing ratio of
10 ClNO₂ vary geographically from below limits of detection to hundreds of ppt (Mielke *et al.*, 2015, Phillips *et al.*,
11 2012, Bannan *et al.*, 2015) and up to 3 parts per billion (ppb) (Tham *et al.*, 2014, Riedel *et al.* 2014, Liu *et al.*,
12 2017) in heavily polluted urban areas. To date, the majority of these measurements have been performed in the
13 United States, with more recent research in Europe, China etc. (Tham *et al.*, 2014, T Wang *et al.*, 2016, X. Wang
14 *et al.*, 2017, Z. Wang, Liu *et al.* 2017). A major factor in the variation of ClNO₂ mixing ratios is the availability
15 and abundance of aerosol chloride which can vary significantly, although is predominantly present as sodium
16 chloride from sea salt.

17 Iodide adduct ionization has previously been applied to measure inorganic halogens in ambient air (Osthoff *et al.*,
18 2008, Riedel *et al.*, 2012, Thornton *et al.*, 2010, Le Breton *et al.*, 2017a) using mass spectrometers with quadrupole
19 mass analysers. This technique involves periodically changing the tuning of the spectrometer to allow transmission
20 of a particular mass ion to the detector. Several species are therefore often “chosen” for detection in order to
21 achieve high enough time resolution. Recent developments and availabilities of a Time of Flight Chemical
22 Ionisation Mass Spectrometer (ToF-CIMS) have enabled the simultaneous measurement of all detectable ions by
23 an ionization technique via high frequency full mass spectral collection. The high resolving power (3500) of this
24 technique also enables much lower limits of detection for species which may have the similar mass to a compound
25 that is much more abundant via multi peak fitting. This technique has previously been applied for the measurement
26 of ClNO₂ and Cl₂ (Faxon *et al.* 2015) and recently for Cl-VOCs (Wang *et al.*, 2017) in the gas phase. In this study,
27 a ToF-CIMS utilizing the FIGAERO (Filter Inlet for Gas and AEROsols) is deployed at a site in semi-rural Beijing,
28 China to measure the gas and particle phase precursor (ClNO₂, N₂O₅) and selective halogen containing species at
29 high time frequency and resolving power to further our understanding of the chlorine atom budget in this region
30 and its potential fate.

31

32 **2. Experimental**

33 **2.1 Site description**

34 The data presented here were collected during the inter-collaborative field campaign, within the framework of a
35 Sino-Sweden research project “Photochemical Smog in China” aimed to further our understanding of the episodic
36 pollution events in China through gas and particle phase measurements with numerous analytical instruments. The
37 laboratory setup in the Changping University Campus of PKU was situated at a semi-rural site 40 km North West

1 of Beijing close to Changping town (40.2207° N, 116.2312° E). The general setup has previously been described
2 by Le Breton *et al.*, 2017b.

3
4 All instruments sampled from inlets setup in a laboratory 12 metres high from the 13th May 2016 to 23rd June 2016.
5 The site has a small town within its vicinity and some small factories within 5 kilometers. A High Resolution Time
6 of Flight Aerosol Mass Spectrometer (HR-ToF-AMS) was utilized to measure the mass mixing ratios and size
7 distributions of non-refractory species in submicron aerosols, including organics, sulfate, ammonium and chloride
8 (DeCarlo *et al.*, 2006, Hu *et al.*, 2013). The setup of this instrument has been previously described by Hu *et al.*,
9 (2016). Photolysis rates were measured by a commercial spectroradiometer for O₃, NO₂, HCHO, HONO and H₂O₂
10 (Metcon UF CCD), the instrument was calibrated by a high power halogen lamp after the field campaign. The
11 photolysis rate of other related species were scaled by the recommendation of the Jet Propulsion Laboratory (JPL)
12 kinetic evaluation report (Burkholder *et al.*, 2015). Before the campaign the was instrument calibrated through
13 comparison with a chemical actinometer utilised in 2014 (Zou *et al.*, 2016), agreeing within 10%. The surface
14 albedo is normally 0.05 at the ground near the site. Upwelling radiation is neglected as is represents an insignificant
15 fraction of the downwelling values.

16 An Ionicon Analytik high sensitivity PTR-MS (Proton TRansfer Mass Spectrometer) as described by de Gouw
17 and Warneke *et al.*, (2007) provided supporting precursor VOC measurements. Detailed information about the PTR
18 MS measurements can be found in Yuan *et al.* 2012 and 2013. In brief, 28 masses are measured throughout the
19 campaign at 1 Hz. Zero air, which was produced by ambient air passing through a platinum catalytic converter at
20 350 °C (Shimadzu Inc., Japan), was measured for 15 min every 2.5 hours to determine the background. Aromatic
21 masses (m/z 79 for benzene, m/z 93 for toluene, m/z 105 for styrene, m/z 107 for C8 aromatics and m/z 121 for
22 C9 aromatics), oxygenated masses (m/z 33 for methanol, m/z 45 for acetaldehyde, m/z 59 for acetone, m/z 71 for
23 MVK+MACR and m/z 73 for MEK), isoprene (m/z 69) and acetonitrile (m/z 42) were calibrated by using EPA
24 TO15 standard from Apel-Riemer Environmental Inc., USA. Formic acid (m/z 47), acetic acid (m/z 61),
25 formaldehyde (m/z 31), and monoterpenes (m/z 81 and m/z 137) were calibrated by permeation tubes (VICI,
26 USA). The uncertainties of most species are below 10%, which is detailed in the previous work (Liu, Y. 2015,
27 ACP).

28 29 **2.2 ToF-CIMS setup**

30 Gas and particle phase ambient species were measured using an iodide ToF-CIMS (resolving power of 3500)
31 coupled to the FIGAERO inlet (Lopez-Hilfiker *et al.*, 2014). The setup for this campaign has previously been
32 described by Le Breton *et al.* (2017b). Briefly, the iodide ionization scheme was utilised to acquire non-fragmented
33 ions of interest by passing UHP N₂ over a permeation tube containing liquid CH₃I (Alfa Aesar, 99%), and through
34 a Tofwerk X-Ray Ion Source type P (operated at 9.5 kV and 150 μA) to produce the iodide reagent ions. The
35 ionized gas was then carried out of the ion source and into the Ion-Molecule Reaction (IMR) chamber, which was
36 heated to 40 degrees Celsius to reduce wall loss, through an orifice (Ø = 1 μm). The inlet lines were 2 metres long
37 and composed of copper tubing (12 mm) for the aerosol inlet and Teflon tubing (12 mm) for the gas sample line.
38 Particles were collected onto a Zefluor® PTFE membrane filter at the same rate as the gas inlet line sampling, 2
39 SLM. The FIGAERO was operated in a cyclic pattern; 25 minutes of gas phase measurement and simultaneous

1 particle collection, followed by a 20 minute period during which the filter was shifted into position over the IMR
2 inlet and the collected particle mass was desorbed.

4 **2.3 Calibration**

5 In the field formic acid calibrations were performed daily utilising a permeation source maintained at 40 °C. A dry
6 N₂ flow (200 sccm) was passed over the permeation source and joined a 2 SLM N₂ flow line directed towards the
7 inlet. The mixing ratio of the flow was determined by mass loss in the laboratory after the campaign. The sensitivity
8 of the ToF-CIMS to formic acid was found to be 3.4 ion counts per ppt Hz⁻¹ for 1x10⁵ iodide ion counts.

9 N₂O₅ was synthesized by mixing 20 ppm O₃ with pure NO₂ (98%, AGA Gas) in a glass vessel and then passing
10 the mixture through a cold trap held at -78.5 °C by dry ice. The N₂O₅ was transferred to a diffusion vial fitted with
11 a capillary tube (i.d. 2 mm). The N₂O₅ diffusion source was held at a constant temperature (-23 °C), and the mass
12 loss rate was characterized gravimetrically for a flow rate of 100 sccm. The same flow was added to a dry nitrogen
13 inlet dilution flow of 2 SLM to calibrate the CIMS. ClNO₂ measurements were quantified by passing the N₂O₅
14 over a wetted NaCl bed to produce ClNO₂. The decrease in N₂O₅ from the reaction with NaCl was assumed to be
15 equal to the mixing ratio of ClNO₂ produced (i.e., a 100% yield). Conversion of N₂O₅ to ClNO₂ can be as efficient
16 as 100% on sea salt, but it can also be lower, for example if ClNO₂ were to convert to Cl₂ (Roberts et al., 2008).
17 For NaCl the conversion efficiency has however been as low as 60% (Hoffman et al., 2003). In this calibration we
18 have followed the accepted methods of Osthoff et al., (2008) and Kercher et al., (2009) that show a conversion
19 yield of 100% and have assumed this yield in the calibrations of this study. The lower detection limit of the CIMS
20 to N₂O₅ and ClNO₂ was found to be 9.5 and 1.2 ppt respectively for 1 minute averaged data. The error in the
21 individual slope of the calibrations results yields a total uncertainty of 30% for both N₂O₅ and ClNO₂. These
22 sensitivities for N₂O₅ and ClNO₂ (9.8 and 1.6 ion counts per ppt Hz⁻¹ for 1 x 10⁵ iodide ion counts) were applied
23 relatively to that of formic acid. The other inorganic halogens reported in this work are reported in ion counts.
24 Other acids identified by CIMS which are reported in the literature are given the sensitivity of N₂O₅ to provide a
25 minimum concentration so no concentrations are over estimated.

26 A post campaign calibration of chloroacetic acid (99%, Sigma Aldrich) was utilised to characterise a sensitivity
27 factor for a Cl-VOC. The calibration was performed using the same method as for formic acid and gave a sensitivity
28 of 1.02 ion counts ppt⁻¹ Hz when normalized to 1 x 10⁵ I⁻ ion counts. This similar sensitivity to that of the Cl VOC
29 to that of ClNO₂ could imply a relative sensitivity may be appropriate to constrain the mixing ratios of all Cl
30 VOCs, although further work is required to confirm this and therefore the manuscript reports all Cl VOC
31 measurements in units of ion counts.

33 **2.4 Model setup**

34 The EMEP MSC-W chemical transport model (Simpson et al., 2012, Simpson et al., 2017) driven by meteorology
35 from the WRF-ARW model (Skamarock et al., 2008) was utilised to support source analysis of the particulate
36 chloride. The model was run on two nested domains (0.5° and 0.1667° resolution respectively) with biomass

1 burning emissions from the two databases FINN and GFAS, and anthropogenic emissions from the MEIC
2 inventory (<http://meicmodel.org/>). Two versions of the model, one getting emissions from open biomass burning
3 from the Fire Inventory from NCAR (FINN) (Wiedinmyer et al., 2011) and one getting them from the Global Fire
4 Assimilation System (GFAS) (Kaiser et al., 2012), were run for the entire period of the Changping measurement
5 campaign.

6 **Results and Discussion**

7 **3.1 Peak identification and quantification**

8 Peak fitting was performed utilizing the Tofware peak fitting software for molecular weights up to 620 AMU. The
9 standard peak shape was fitted a peak on the spectra until the residual was less than 5%. Each unknown peak was
10 assigned a chemical formula using the peaks exact mass maxima to 5 decimal places and also isotopic ratios of
11 subsequent minor peaks. An accurate fitting was characterized by a ppm error of less than 5 and subsequent
12 accurate fitting of isotopic peaks. The analysis here focuses on species identified in the mass spectra considered to
13 possibly play important roles with respect to the night-time chlorine reservoir and several other key night-time
14 oxidants; ClNO₂, HCl, Cl₂, ClO, HOCl, OClO, ClONO₂, N₂O₅ and Cl-VOCs. Figure 1 displays the average mass
15 spectra for the measurement campaign and the peak fitting applied for ClO and ClNO₂. All species were
16 represented by a dominant peak with a multi peak fit, although a number of co-existing peaks were present for
17 much of the campaign. This signifies the importance of high resolution fit data and the need for high resolution
18 measurements. A quadrupole CIMS may not be able to resolve the peak adjacent to ClO at m/z 178 (dominant
19 peak is IC₆F₃HO₃⁻) and the second dominant peak for the ClNO₂ fit (cluster of HNO₃ with water) would result in
20 a 10% over estimation.

21

22 **3.2 N₂O₅ measurements**

23 The CIMS and a Cavity Enhanced Absorption Spectrometer (CEAS) measured N₂O₅ (Wang *et al.*, 2017)
24 simultaneously from the 13th May 2016 to the 6th June 2016. However, given the use of the FIGAERO, the CIMS
25 alternated measurements between gas and particle phases so did not generate a completely continuous gas phase
26 time series. Here, the CEAS is utilised to validate the CIMS N₂O₅ (at m/z 235) measurements and also instrument
27 stability. The CEAS utilised a dynamic source by mixing NO₂ and O₃ to generate stable N₂O₅ for calibration (Wang
28 *et al.*, 2017). The source was used to calibrate the ambient sampling loss of N₂O₅ in the sampling line, filter, the
29 preheater cavity and optical cavity. This was performed pre and post campaign. During the campaign the
30 reflectivity of the high reflectivity mirror was calibrated daily and filter changed hourly. The simultaneous
31 measurements of N₂O₅ can be shown in Figure 2 for one minute averaged data. The time series shows good
32 agreement for both background mixing ratios during the day (sub 10 ppt) and high night-time mixing ratios (up to
33 800 ppt), excluding one night. The highest N₂O₅ levels observed by both the CEAS and CIMS were observed on
34 the 3rd June although the CEAS reports 880 ppt whereas the CIMS reports 580 ppt. If included in the analysis the
35 R² is 0.71 and when excluded it is 0.76. To date the reason for this deviation during that night is not known but it
36 should be stressed that N₂O₅ measurements are delicate and highly dependent on sampling condition, e.g. the RH.
37 Nevertheless, excluding this night from the comparison, a slope of 0.85 is observed and an offset of 0.9 ppt. The

1 diurnal profile in Figure 2 represented the difference between the two measurements throughout the campaign.
2 The largest error between the two measurements occurs at night during the higher levels of N_2O_5 , although
3 averaging at 4 ppt (representing 11% error on the average campaign concentration). Differences could arise from
4 a number of various factors. Inlet differences such as the CIMS heated IMR (to 40 °C to reduce wall loss), residence
5 time and ambient NO_2 can all change thermal decomposition and wall loss rates between the instruments, which
6 is determined for the CEAS in Wang *et al.* (2017) but not for the CIMS in this work. Also, the separate inlets were
7 facing in different directions within the same laboratory, possibly enabling local wind patterns to affect the mixing
8 ratios reaching each instrument.

9 The CEAS data was further utilised to assess any sensitivity changes for the CIMS that daily carboxylic acid
10 calibrations did not account for. A time series of hourly factor differences between the CIMS and CEAS was
11 implemented into these data to weight the measurements to a normalised sensitivity. The high level of agreement
12 (R^2 of 0.76) from low mixing ratio measurements and a species with a short lifetime from different inlets confirms
13 the accuracy and reliability of the CIMS measurements for this campaign.

14 Generally, N_2O_5 was detected throughout the campaign with a clear diurnal variation peaking at night-time and
15 rapidly falling to below limits of detection in the daytime as a result of photolysis of N_2O_5 and NO_3 . The campaign
16 mean night-time mixing ratio was 121 ppt with a standard deviation of 76 ppt. The maximum mixing ratio of N_2O_5
17 observed was 880 ppt on the 3rd June. This range of mixing ratios lie within the recently reported values in the
18 literature, but not at the extreme mixing ratios as observed in Germany (2.5 ppb) (Phillips *et al.*, 2016) or Hong
19 Kong (7.7 ppb) by Wang *et al.* (2016) and Brown *et al.* (2017). Although the mean mixing ratios do not increase
20 significantly during the pollution episodes, the maximum mixing ratios detected overnight increase by up to a
21 factor of 4. Further analysis of N_2O_5 nighttime chemistry was performed by Wang *et al.* (2018) who calculated an
22 average steady state lifetime of 310 ± 240 s and mean uptake coefficient of 0.034 ± 0.018 .

23

24 **3.3 Inorganic chlorine: Abundance, profiles and source**

25 **3.3.1 Abundance and profiles**

26 Mean diurnal profiles of HCl, Cl_2 , ClONO_2 , HOCl, ClO and ClNO_2 are displayed in Figure 3 from data between
27 the 23rd May and the 6th June. HCl exhibited a standard diurnal profile increasing in mixing ratio throughout the
28 day and peaking at 4 pm which then fell off slowly at night. The mean HCl campaign mixing ratio was 510 ppt
29 (standard deviation (σ) 270 ppt) and the maximum HCl mixing ratio was 1360 ppt on the 30th June. Cl_2 exhibited
30 a diurnal profile peaking at both night-time and daytime. High mixing ratios were observed at night followed by a
31 sharp loss at sunrise and a general build-up throughout the day. The campaign mean mixing ratio was 0.65 ppt (σ
32 0.5 ppt) and the maximum mixing ratio was 4.2 ppt on the 4th June just before midnight. This agrees well with
33 recent urban measurements of Cl_2 in the USA where Faxon *et al.* (2015) observed a maximum of 3.5 ppt and Finley
34 *et al.* (2006) observed up to 20 ppt in California. Up to 500 ppt Cl_2 has recently been reported in the Wangdu
35 County, South West of Beijing (Liu *et al.*, 2017). Although the mixing ratios we report here are significantly lower,
36 as detailed later, their source may be of similar origin, which is indicated to be from power plant emissions.

1 The diurnal profile of HOCl peaked during the daytime via its main formation pathways are via reaction of ClO
2 and HO₂ and Cl with OH. Interestingly, the ClO in this work exhibits a night-time diurnal peak, contradicting
3 known formation pathways via Cl reaction with O₃ and the photolysis of ClONO₂. The complexity continues as
4 ClONO₂ also peaks during the night, given that its main known formation pathway is via reaction of ClO (produced
5 at sunrise via ClNO₂ photolysis) with NO₂. The misidentification of ClONO₂ and ClO is not thought to be a
6 possible reason for these discrepancies due to the low number of mass spectral peaks that have maxima at night
7 and the mass defect of chlorine making the peak position unique to chlorine containing molecules. IMR chemistry
8 is also not a possible source as these reactions would occur throughout the day, therefore skewing all of the data
9 and not just the night-time levels, although there is a possibility that ClONO₂ can be formed in the IMR by reactions
10 between ClO and NO₂. It is hypothesized that in extremely high OH and HO₂ mixing ratios, all ClO is rapidly
11 converted to HOCl, limiting the formation on significant levels of ClO and subsequently ClONO₂. Khan et al
12 (2008) suggest that Cl atoms of around 2×10^4 molecules cm⁻³ could be present at night via analysis of alkane
13 relative abundance. Although a formation mechanism is not proposed, it provides further evidence that ClO
14 formation at night-time is possible and may represent an unknown reaction pathway, which would agree with the
15 measurements presented in this work.

16 ClNO₂ exhibited a similar diurnal profile as N₂O₅, peaking at night-time and lost during daylight due to photolysis.
17 The campaign mean night-time mixing ratio was 487 ppt. The maximum mixing ratio observed was 2900 ppt on
18 the 31st May, similar to that previously measured at semi-rural site in Wangdu (up to 1500 ppt) (Liu et al., 2017),
19 Mount Tai (2000 ppt) (Wang et al., 2017), but lower than that in Hong Kong (4 ppb) (Wang et al 2016).

20

21 3.3.2 Source of chloride

22 The high levels of ClNO₂ indicate a local significant source of chlorine to support these observations. The
23 dominant source of chlorine atoms for ClNO₂ production within models, such as the Master Chemical Mechanism
24 (MCM), is from sea salt. However, the site is situated 200 km from the Yellow Sea and therefore this origin would
25 have a low probability. The mean AMS chloride mass loading was 0.05 μg m⁻³ for the campaign with a maximum
26 of 1.7 μg m⁻³. The Cl⁻ from the AMS appears to be correlated strongly with CO and SO₂, possibly originating from
27 power plants or combustion sources. It should be noted that the AMS data does not include refractory aerosol and
28 also has a cut off size larger than the anticipated size of sea salt particles. Instead, the high Cl⁻ observed appears to
29 originate from mainland areas to the site (Figure 4) rather from the nearest coast, further supporting a
30 anthropogenic source. Tham et al., (2016) observed a strong correlation of aerosol chloride with SO₂ and potassium
31 from measurements done during the same season in 2014 at Wangdu (semi-rural site 160 km south West of
32 Beijing) and suggested contributions to fine chloride from burning of coal and crop residues. The latter was also
33 supported by satellite fire spot count data (Tham et al., 2016). Riedel et al. (2013) have previously reported high
34 ClNO₂ mixing ratios observed from urban and power plant plumes measuring high mixing ratios of gas phase Cl₂.
35 The correlation with SO₂ indicates coal burning as a potential source of particulate chlorine which is known to be
36 a significant source of PM in the Beijing region (Ma et al., 2017), and the correlation with CO and benzene could
37 be an indicator of biomass burning (Wang et al., 2002). To support this analysis, figure S1 displays a wind rose
38 plot in which radial and tangential axes represent the wind direction and speed (km h⁻¹). The colour bar represents

1 the PM_{2.5} concentration. We could see that during the campaign, the severe pollution was from the south and
2 southwest, with little contribution from the east part. Therefore, it is likely that little contribution of the chloride
3 was from the ocean.

4 In order to test the hypothesis of biomass burning as a source of particulate chlorine, biomass burning emissions
5 and transport utilising the EMEP MSC-W chemical transport model driven by meteorology from the WRF-ARW
6 model (Skamarock et al., 2008) were used. Neither of the two biomass burning databases used (FINN and GFAS)
7 contained data on chlorine emissions, so instead the biomass burning emissions of CO (CO_{bb}) were tracked and
8 compared with the total mixing ratio of CO (CO_t) at the Changping site. CO was chosen since the measurements
9 at Changping had shown a strong correlation between CO and ClNO₂ and because CO could be expected to be co-
10 emitted with chlorine for both biomass burning and industrial combustion.

11 Figure S2 (supplementary) shows the time series of the measured ClNO₂ mixing ratios at the Changping site, as
12 well as the modelled mixing ratios of CO_t and CO_{bb}. CO_{bb} is shown for calculations using either the FINN or the
13 GFAS data base, while for clarity the CO_t is only shown using the FINN data base. It is clear that mixing ratios of
14 CO_{bb} are very low compared with CO_t (figure S2). The two pollution episodes on May 18-May 23 and May 28-
15 June 5, are to some extent visible in all time series, but for the biomass burning CO series, the second episode is
16 much less pronounced. Night-time averages of the mixing ratios shown in figure S2 were calculated for each night
17 for the time period 18:00 to 08:00 local time (UTC+8), roughly corresponding to the period when ClNO₂ is not
18 destroyed by photolysis. Nights with significant amount of missing data for the measurements were excluded.
19 Figure S2 shows scatter plots of these averages of ClNO₂ against the averages of the other species including their
20 linear fits. The R² value for these fits were 0.48, 0.04, and 0.21 for CO_t, CO_{bb} FINN, and CO_{bb} GFAS
21 respectively. The fact that mixing ratios of CO_{bb} are so much smaller than CO_t according to the model, combined
22 with the much better correlation for CO_t than for CO_{bb} strongly suggests that industrial emissions are the dominant
23 source of chlorine, rather than biomass burning. To further investigate the source of chloride, the model was also
24 run to calculate sea salt levels instead of CO. This resulted in a poor correlation between sea salt and the ClNO₂
25 (figure S4). The absolute levels of sea salt calculated by the model were also very low, unlikely to be able to
26 produce the observed mixing ratios of ClNO₂ as observed by CIMS.

27

28 **3.4 Particle phase ClNO₂**

29 A particle desorption profile was observed in the high resolution data for ClNO₂. The count increase at this 1 AMU
30 mass can be attributed to two sources; SO₃ and ClNO₂ as shown in Figure 5. The SO₃ peak is predominantly found
31 in the particle phase and is below the limit of detection (LOD) in the gas phase. During initial analysis of these
32 data, SO₃ interfered with the ClNO₂ peak fitting and attributed its counts to ClNO₂ in the particle phase as its ³³S
33 ion is only 0.005 AMU away from the ClNO₂ peak. Upon its inclusion into the peak list and utilisation of the
34 Tofware feature which constrains isotopes and reallocates the signal appropriately, ClNO₂ remains to indicate a
35 strong desorption profile. The diurnal cycle of these desorptions correlate well with the ClNO₂ gas phase profile,
36 indicating a correct assignment of the counts to particle phase ClNO₂. The desorption profiles with respect to
37 temperature also exhibit a thermogram structure and not for example a gas phase leak into the system which could
38 have accounted for the correlation with the gas phase time series. This suggests the possible presence of ClNO₂ in

1 the particle phase. Another possible explanation could be the deposition of ClNO₂ from the gas phase onto the
2 filter as the ambient air flows through the FIGAERO.

3 If we assume the analysis and collection technique is correct, we see an average particle to gas phase partitioning
4 of 0.07, with a maximum of 0.33 and a minimum of 0.009. The average mixing ratio of ClNO₂ collected onto the
5 filter during desorption is 13 ppt with a maximum of 120 ppt. Previous modelling studies assume all ClNO₂ is in
6 the gas phase due to the low Henry's law constant e.g. for the TexAQS II campaign they calculated that 0.1 ppb
7 in the gas phase would yield 0.54 ppt in the particle phase (Simon *et al.*, 2008). However, these data suggest that
8 a non-negligible amount of the chlorine associated with ClNO₂ is not liberated from the particle phase, assuming
9 that no additional ClNO₂ is formed by thermally driven reactions. The slope of the particle to gas phase CIMS data
10 is calculated to be 0.048, a factor of 96 higher than using the Henry's law coefficient to estimate the particle mixing
11 ratio.

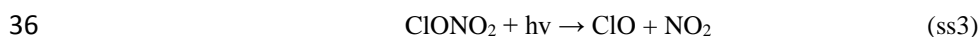
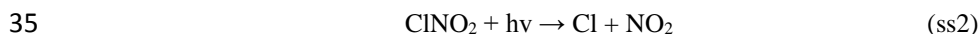
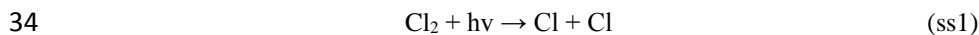
12

13 3.5 ClNO₂ daytime persistence and Cl liberation

14 Both ClNO₂ and N₂O₅ are photolytically unstable, with studies reporting lifetimes on the order of hours for ClNO₂
15 depending on the solar strength (e.g. Ganske *et al.*, 1992, Ghosh *et al.*, 2011). Nocturnal ClNO₂ removal pathways
16 have generally been reported to be negligible, with ClNO₂ being assumed to be relatively inert (Wilkins *et al.*,
17 1974; Frenzel *et al.*, 1998; Rossi, 2003; Osthoff *et al.*, 2008), but the work of Roberts *et al.*, (2008) and Kim *et al.*,
18 (2014) would suggest that this may not be strictly true. However, given that the average diurnal profile does not
19 show the importance of nocturnal removal pathways in this study, observed losses are attributed solely to
20 photolysis, with J(ClNO₂) controlling the lifetime.

21 Rapid photolysis can be observed for N₂O₅ in Figure 6 showing a near instant drop below LOD, whereas the ClNO₂
22 mixing ratio not only persists for up to 7 hours, but also shows evidence of an increase in mixing ratio at 7 am
23 (Figure 6). This is observed throughout the campaign and has been frequently observed in the previous study at
24 Wangdu (Tham *et al.*, 2016). The breakdown of the nocturnal boundary layer and inflow of air masses from above,
25 carrying pollution from nearby industry/ies is a likely cause of this persistence of possible increase of ClNO₂. Liu
26 *et al.* (2017) also observed high daytime mixing ratios of ClNO₂ (60 ppt) at the Wangdu site which they attribute
27 to a possible oxidation mechanism due its correlation with O₃ and Cl₂ providing a daytime formation pathway to
28 maintain mixing ratios against its rapid photolysis.

29 Consistent with past measurements and the measurements of this study, ClNO₂ is expected to provide a significant
30 source of Cl during day time hours, presenting a potentially significant source of the reactive Cl atom during the
31 day. Its rapid photolysis rate and elevated mixing ratios enables Cl to compete with OH oxidation chemistry, the
32 known dominant daytime radical source. Here, a simple steady state calculation will be used to determine the Cl
33 atom mixing ratio summarised as follows, but detailed within the supplementary:



1 Although this study does not reach the scope of characterising O₃ and RO_x production from chlorine atom
2 chemistry, statistics are often reported with ClNO₂ morning chemistry via modelling simulations, we can put into
3 perspective the mean and maximum mixing ratios relative to other studies. Tham *et al.* (2016) recorded a maximum
4 ClNO₂ mixing ratio of 2070 ppt from a plume originating from Tianjin, the closest megacity to Beijing, and report
5 a 30% increase in RO_x production and up to 13% of O₃ production. Liu *et al.* (2017) observed peak mixing ratios
6 up to 3 ppb and similar diurnal mixing ratios which they calculated contributes to a 15% enhancement of peroxy
7 radicals and 19% O₃ production. Wang *et al.* (2016) report up to 4.7 ppb of ClNO₂ in Hong Kong and calculated
8 a maximum increase of 106% of HO_x in the morning and an enhancement of O₃ production the next day by up to
9 41%. Therefore, it is evident that this work supports similar studies in Asia that conclude that chlorine atom
10 oxidation significantly contributes to atmospheric oxidation via RO_x and O₃ production. Although several studies
11 have demonstrated a non-negligible impact of chlorine oxidation chemistry (e.g. Oshoff *et al.*, 2008, Riedel *et al.*,
12 2014 and Sarwar *et al.*, 2014), the impact of Cl chemistry varies significantly between various areas and
13 atmospheric conditions, e.g. Bannan *et al.*, (2015, 2017) deemed the impact from chlorine atom chemistry to be
14 relatively low with respect to O₃ production and competing with OH radicals for VOC oxidation.

15

16 **3.6 VOC oxidation by chlorine atoms**

17 Steady state calculations of OH (as described by Whalley *et al.*, 2010) estimate that campaign average maximum
18 mixing ratio was 7×10^6 molecules cm³ (Figure 7b), 6 times greater than the maximum chlorine atom mixing ratio
19 and 14 times higher than the average chlorine atom mixing ratio. Pszenny *et al.* (2007) report estimated OH to
20 chlorine atom ratios, from VOC lifetime variability relationships, of 45 to 199 along the East Coast of the United
21 States. Although the ratio appears much larger than calculated in this work, here we present not only significantly
22 higher mixing ratios of ClNO₂ which are appearing to be a consistent conclusion from measurements in Asia, but
23 also the chlorine within this study appears to originate from an anthropogenic origin rather than marine, possessing
24 the ability to supply a much larger reservoir of halogens to be liberated through photolysis.

25 The relative oxidation rate of the chlorine atom and OH to VOCs can vary greatly. Rate coefficients for reaction
26 of Cl atoms with some volatile organic compounds have been shown to be up to 200 times faster than the
27 comparable reaction with OH. The ratio reported here is significantly less than this each day, Cl can subsequently
28 dominate VOC oxidation for some fraction of the day. Here, the diurnal maxima of the chlorine atom and OH
29 differs by 5 hours, enabling chlorine atoms to dominate VOC oxidation earlier in the day before OH mixing ratios
30 have built up. The relative oxidation rate of VOCs to OH and the chlorine atom also varies greatly, creating a
31 difference for various VOCs. If an average reaction rate for alkenes and alkanes to Cl and OH is calculated, it is
32 possible to generalise the significance of each oxidation pathway to qualitatively assess the contribution chlorine
33 atoms have on oxidation chemistry. It can be seen in Figure 8 that alkenes are much more likely to be oxidised by
34 OH than Cl, although a significant contribution (15%) is attributed to chlorine chemistry. Although significant if
35 evaluated on a global level, Liu *et al.*, (2017) estimated that Cl atoms oxidize slightly more alkanes than OH
36 radicals in a similar region of China, implying the increased scale of chlorine oxidation in China. Alkanes are
37 known to have a much higher Cl to OH relative reaction rate than alkenes and Cl contribution to oxidation is higher
38 than OH until midday. The contribution to oxidation remains almost equal for the remainder of the day due to the

1 persistence of ClNO₂ and also relatively high levels of Cl₂ and HCl. This analysis is representative of that by
2 Bannan *et al.* (2015) who report contributions of alkene and alkane oxidation by Cl up to 3 and 15% respectively
3 from ClNO₂ mixing ratios peaking at 724 ppt.

4 This significant oxidation of VOCs by chlorine atoms will result in different products to that of OH oxidation as
5 illustrated and that neglecting the contributions made by Cl atoms will significantly underestimate the degree of
6 chemical processing of VOCs in this study, and other environments where there is a source of Cl atoms. Evidence
7 of the proposed Cl oxidation of VOCs is validated through detection of selected Cl induced oxidation products by
8 the ToF-CIMS, all of which are displayed in Table 1.

9

10 **3.6.1 Isoprene oxidation by the chlorine atom**

11 1-Chloro-3-methyl-3-butene-2-one (CMBO, C₅H₆ClO), a unique marker of chlorine chemistry, has previously
12 been measured at mixing ratios up to 9 ppt by offline gas chromatography in Houston Texas (Tanaka *et al.*, 2003)
13 and in laboratory studies of chlorine-isoprene oxidation (Wang *et al.* (2017)). CMBO exhibited a campaign
14 maximum of 21 and mean of 34 ion counts (near similar ppt mixing ratio if the chloroacetic acid calibration
15 sensitivity is applied) exhibiting a near typical diurnal profile with abundance rising sharply after sunrise, at the
16 same rate as the chlorine atom production but maintaining mixing ratios past noon longer than that of isoprene and
17 the chlorine atom.

18 The daily maxima of CMBO varied throughout the campaign and can be explained by the relative mixing ratios
19 of its precursors; the chlorine atom and isoprene. Its mixing ratio throughout the campaign followed similar
20 intensities to its precursors and figure 9 highlights its dependence on both Cl atom and isoprene mixing ratios. The
21 production rate of Cl and mixing ratio of isoprene were relatively low from the 24th to the 27th of May (1.6 x 10⁵
22 molecules cm⁻³ s⁻¹ Cl and 0.5 ppb isoprene), which resulted in relatively low CMBO mixing ratios. An increase in
23 isoprene and Cl on the 28th to the 30th May was subsequently mirrored by the CMBO levels as qualitatively
24 expected. On closer inspection of the 30th and 31st May, the mixing ratio of CMBO was lower than expected on
25 the 30th due to higher chlorine atom and isoprene mixing ratios compared with the 31st. This could be explained
26 by anticipated higher OH mixing ratio as calculated by the steady state model, which is also further represented
27 by higher mixing ratios of IEPOX (isoprene epoxydiols, i.e. OH oxidation products) on the 30th. This illustrates
28 how the ToF-CIMS can identify isoprene oxidation products of two competing oxidation pathways. The high
29 levels of IEPOX on the 28th May can also possibly describe the relatively high levels of CMBO in the particle
30 phase due to an already well oxidised air mass. CMBO may also not be unique to only isoprene-chloride reactions
31 and therefore have alternative sources not represented in this data set.

32 Further daily oxidation rates can be probed via analysis of the related isoprene oxidation products observed by the
33 CIMS. Figure 10 depicts the diurnal time series of the precursor itself and several Cl-VOC products and IEPOX.
34 CMBO mixing ratios rise rapidly after sunrise due to the low mixing ratio of OH and high production rate of the
35 chlorine atom. The secondary and tertiary products, C₅H₉ClO₂ and C₅H₉ClO₃ (also measured in the laboratory by
36 Wang *et al.*, 2017) increased in mixing ratio at a much slower rate, but appear to peak later in the day (4 pm)
37 whereas CMBO peaked around 10 am (similar to the ClNO₂ peak time) and fall off, due to its further oxidation to

1 form the secondary and tertiary products. IEPOX mixing ratios increased slowly after sunrise and peaked later in
2 the day, as expected due to the availability of OH and competition from the chlorine atom chemistry. The similar
3 time series of the secondary and tertiary products to IEPOX was also reported by Wang *et al.*, (2017) and were
4 suggested to be ideal tracers of SOA production.

5

6 **3.6.2 Anthropogenic Cl-VOC production**

7 A similar unique chlorine oxidation marker in urban coastal areas, has been reported in the literature for 1, 3
8 butadiene; 4-chlorocrotonaldehyde (CCA) (Wang *et al.*, 2000). No measurements of 1, 3 butadiene were made
9 during this field campaign, although due to its common source to benzene (automobile exhausts (Ye *et al.*, 1998),
10 we present a comparison of the CCA measured by CIMS and benzene measurements made by the PTR-MS. The
11 intensity of CCA in both the gas and particle phase reflect well the abundance of its precursors. The maximum
12 mixing ratio of the chlorine atom coincides with a high mixing ratio of benzene and subsequently CCA on the 30th
13 May whereas very low levels of CCA were observed for the beginning of the campaign (Figure 11).

14 The diurnal time series of benzene (Figure 12) indicates high mixing ratios in the early hours of the day, possibly
15 associated with high anthropogenic activity or an inflow of urban air masses from downtown Beijing. The mixing
16 ratio falls off throughout the day and almost perfectly anti correlates with the CCA gas phase diurnal profile which
17 increases from sunrise and peaks at 3 pm. The particle phase CCA diurnal time series steadily builds up throughout
18 the day and does not peak until late in the evening, providing evidence of SOA production from the chlorine
19 oxidation of anthropogenic pollutants.

20

21 **4. Conclusions**

22 A FIGAERO ToF-CIMS was utilised in Beijing to assess the liberation of chlorine atoms via inorganic halogen
23 photolysis. A suite of inorganic halogens were detected, namely ClNO₂ reaching mixing ratios up to 2900 ppt,
24 which is suggested to have an anthropogenic origin due to the particulate chlorine correlation with SO₂, benzene
25 and CO. ClNO₂ was identified in the particle phase at higher ratios with respect to its gas phase component than
26 expected, which may only prove to be significant at such elevated mixing ratios as observed in East Asia. ClNO₂
27 mixing ratios above LOD persisted up to 7 hours past sunrise, attributed to the lifetime of ClNO₂ at these high
28 mixing ratios and a possible in-flow of heavily polluted air masses from the downtown urban area. Supporting Cl₂
29 and HCl mixing ratios proved to be significant contributors to chlorine atom production via steady state
30 calculations. Compared with data attained from European based campaigns, these mixing ratios exceed marine
31 and urban environments by at least an order of magnitude.

32 This high mixing ratio of chlorine atoms resulted in a steady state calculated OH:Cl ratios down to a factor of 6,
33 suggesting Cl chemistry may be able to dominate alkane oxidation until midday but contribute significantly to
34 alkene oxidation throughout the day (15% on average). This enabled significant mixing ratios of Cl-VOCs to be
35 formed providing the first ambient high time resolution measurements of specific Cl-VOC species simultaneously
36 measured in the gas and particle phase. The measured unique markers of chlorine chemistry for both biogenic and

1 anthropogenic precursors provides quantitative and qualitative data to probe the extent of chlorine atom chemistry
2 and how they compete with OH. Simultaneous measurements of the VOC precursors via PTR-MS, and IEPOX,
3 Cl-VOCs with the CIMS provides rich information on SOA formation pathways via both OH and chlorine atom
4 oxidation. Multistep oxidation products of Cl-VOCs were also identified and can provide partitioning information
5 and SOA formation rates and lifetimes.

6 The results highlight deficiency in chlorine atom chemistry descriptions within models possibly due to a lack in
7 quantification and identification of Cl-VOC products in gas and particle phase. This work provides instrumental
8 capability to probe the competition between OH and Cl oxidation chemistry and quantify their effect on ozone and
9 SOA formation.

10 **Acknowledgement:**

11 The work was carried out under the framework research program on ‘Photochemical smog in China’ financed by
12 Swedish Research Council (639-2013-6917). The National Natural Science Foundation of China (21677002) and
13 the National Key Research and Development Program of China (2016YFC0202003) also helped fund this work.
14

15 **References**

16 Allan, W., Struthers, H. and Lowe, D. C.: Methane carbon isotope effects caused by atomic chlorine in the marine
17 boundary layer: Global model results compared with southern hemisphere measurements. *J. Geophys. Res.* 112,
18 2007.

19 AQIRP, 1995, Effects of gasoline T50, T90 and sulfur on exhaust emissions of current and future technology
20 vehicles. Auto/Oil Air Quality Improvement Research Program, Technical Bulletin No. 18.

21 Baker, A. K., Sauvage, C., Thorenz, U. R., van Velthoven, P., Oram, D. E., Zahn, A., Berninkmeijer, C. A. M.
22 and Williams, J.: Evidence for strong, widespread chlorine atom chemistry associated with pollution outflow
23 from continental Asia, *Sci. Rep.*, 6, 36821, 2016.

24 Bannan, T. J., Booth, A. M., Bacak, A., Muller, J. B. A., Leather, K. E., Le Breton, M., Jones, B., Young, D., Coe,
25 H., Allan, J., Visser, S., Slowik, J. G., Furger, M., Prevot, A. S. H., Lee, J., Dunmore, R. E., Hopkins, J. R.,
26 Hamilton, J. F., Lewis, A. C., Whalley, L. K., Sharp, T., Stone, D., Heard, D. E., Fleming, Z. L., Leigh, R.,
27 Shallcross, D. E., and Percival, C. J.: The first UK measurements of nitryl chloride using a chemical ionization
28 mass spectrometer in central London in the summer of 2012, and an investigation of the role of Cl atom oxidation,
29 *J. Geophys. Res. Atmos.*, 120, 5638–5657, 2015.

30 Bannan, T. J., Bacak, A., Le Breton, M., Ouyang, B., Flynn, M., McLeod, M., Jones, R., Malkin, T. L., Whalley,
31 L. K., Heard, D. E., Bandy, B., Khan, A., Shallcross, D. E., and Percival, C. J.: Ground and airborne U.K.
32 measurements of nitryl chloride, an investigation of the role of Cl atom oxidation at Weybourne Atmospheric
33 Observatory, *J. Geophys. Res. Atmospheres*, 10.2017.

34 Brown, S. S. & Stutz, J. Nighttime radical observations and chemistry *Chem. Soc. Rev.*, The Royal Society of
35 Chemistry, 41, 6405-6447, 2012.

36 Burkholder, J.B. et al. Chemical Kinetics and Photochemical Data for Use in Atmospheric Studies: Evaluation
37 Number 18. Jet Propulsion Laboratory, California Institute of Technology, Pasadena, CA, 2015.

38 Cai, X., Ziemba, L. D. and Griffin, R. J.: Secondary aerosol formation from the oxidation of toluene by chlorine
39 atoms, *Atmos. Environ.*, 42, 32, 2008.

- 1 Brown, S. S., Stark, H., and Ravishankara, A. R.: Applicability of the steady state approximation to the
2 interpretation of atmospheric observations of NO₃ and N₂O₅, *J. Geophys. Res.- Atmos.*, 108, 4539, 2003.
- 3 Brown, S. S., Dube, W. P., Tham, Y. J., Zha, Q. Z., Xue, L. K., Poon, S., Wang, Z., Blake, D. R., Tsui, W., Parrish,
4 D. D., Wang, T.: Nighttime chemistry at a high altitude site above Hong Kong, *J. Geophys. Res. Atmos.*, Vol. 121,
5 Issue. 5, 2457-2475, 2016.
- 6
- 7 DeCarlo, P. F., Kimmel, J., Trimborn, A., Northway, M., Jayne, J. T., Aiken, A., Gonin, M., Fuhrer, K., Horvath,
8 T., Docherty, K., Worsnop, D. R., and Jimenez, J. L.: Field-deployable, high-resolution, time-of-flight Aerosol
9 Mass Spectrometer, *Anal. Chem.*, 78, 8281–8289, 2006.
- 10 de Gouw, J. and Warneke, C.: Measurements of volatile organic compounds in the earth's atmosphere using
11 proton-transferreaction mass spectrometry, *Mass Spectrom. Rev.*, 26, 223–257, 2007.
- 12 Faxon, C. B., Bean, J. K., and Ruiz, L. H.: Inland Mixing ratios of Cl₂ and ClNO₂ in Southeast Texas suggest
13 chlorine chemistry significantly contributes to atmospheric reactivity, *Atmosphere*, 6, 1487–1506, 2015.
- 14 Finley, B. D. and Saltzman, E. S: Measurement of Cl₂ in coastal urban air, *Geophys. Res. Lett.*, 33, 2006.
- 15 Fraser, M. P., G. R. Cass, B. R. Simoneit, & R. A. Rasmussen (1997). Air quality model evaluation data for
16 organics. 4. C2-C36 non-aromatic hydrocarbons. *Environmental science & technology*, 31(8), 2356-2367
17 DOI: 10.1021/es960980g
- 18 Hoffman, R. C., Gebel, M. E., Fox, B. S., and Finlayson-Pitts, B. J.: Knudsen cell studies of the reactions of
19 N₂O₅ and ClONO₂ with NaCl: Development and application of a model for estimating available surface areas and
20 corrected uptake coefficients, *Phys. Chem. Chem. Phys.*, 5, 9, 1780–1789, 2003.
- 21 Hofzumahaus, Andreas, Franz Rohrer, Keding Lu, Birger Bohn, Theo Brauers, Chih-Chung Chang, Hendrik
22 Fuchs, et al. "Amplified Trace Gas Removal in the Troposphere." *Science* 324, no. 5935 (2009): 1702.
- 23 Hu, W. W., Hu, M., Yuan, B., Jimenez, J. L., Tang, Q., Peng, J. F., Hu, W., Shao, M., Wang, M., Zeng, L. 74 M.,
24 Wu, Y. S., Gong, Z. H., Huang, X. F., and He, L. Y.: Insights on organic aerosol aging and the influence of
25 coal combustion at a regional receptor site of central eastern China, *Atmos. Chem. Phys.*, 76 13, 10095-10112,
26 2013.
- 27 Hu, W., Hu, M., Hu, W., Jimenez, J. L., Yuan, B., Chen, W., Wangm M., We, Y., Chen, C., Wang, Z., Peng, J.,
28 Zeng, L. and Shao, M. Chemical composition, sources, and aging process of submicron aerosols in Beijing:
29 Contrast between summer and winter, *J. Geophys. Res.*, 121, 4, 1955-1977, 2016.
- 30 Huang, M., Liu, X., Hu, C., Guo, X., Gu, X., Zhao, W., Wang, Z., Fang, L. and Zhang, W.: Aerosol laser time-of-
31 flight mass spectrometer for the on-line measurement of secondary organic aerosol in smog chamber, *Meas. J. Int.*
32 *Meas. Confed.*, 55(3), 394–401, 2014.
- 33 Keil, A. and Shepson, P.: Chlorine and bromine atom ratios in the springtime Arctic troposphere as determined
34 from measurements of halogenated volatile organic compounds, *J. Geophys. Res.*, 111, 2006.
- 35 Kaiser, J. W., Heil, A., Andreae, M. O., Benedetti, A., Chubarova, N., Jones, L., Morcrette, J.-J., Razinger, M.,
36 Schultz, M. G., Suttie, M., and van der Werf, G. R. (2012). Biomass burning emissions estimated with a global
37 fire assimilation system based on observed fire radiative power. *Biogeosciences*, 9:527-554.
- 38 Kercher, J. P., Riedel, T. P., and Thornton, J. A.: Chlorine activation by N₂O₅: simultaneous, in situ detection of
39 ClNO₂ and N₂O₅ by chemical ionization mass spectrometry, *Atmos. Meas. Tech.*, 2, 193–204, doi:10.5194/amt-
40 2-193-2009, 2009.
- 41 Khan, M. A. H., Ashfold, M. J., Nickless, G., Martin, D., Watson, L. A., Hamer, P. D., Wayne, R. P., Canosa-
42 Mas, C. E. and Shallcross, D. E.: Night-time NO₃ and OH radical mixing ratios in the United Kingdom inferred
43 from hydrocarbon measurements, *Atmos. Sci. Lett.*, 9, 3, 140-146, 2008.

1 Kim, M. J., Farmer, D. K. and Bertram, T. H.: A controlling role for the air–sea interface in the chemical
2 processing of reactive nitrogen in the coastal marine boundary layer, *PNAS*, 111 (11), 2943–3948, 2014.
3

4 Lopez-Hilfiker, F. D., Mohr, C., Ehn, M., Rubach, F., Kleist, E., Wildt, J., Mentel, Th. F., Lutz, A., Hallquist, M.,
5 Worsnop, D., and Thornton, J. A.: A novel method for online analysis of gas and particle composition: description
6 and evaluation of a Filter Inlet for Gases and AEROSols (FIGAERO), *Atmos. Meas. Tech.* 2014, 7, 983–1001,
7 doi:10.5194/amt-7-983-2014.

8 Le Breton, M, Bannan, T. J., Shallcross, D. E., Khan, M. A., Evans, M. J., Lee, J., Lidster, R., Andrews, S.,
9 Carpenter, L., Schmidt, J., Jacob, D., Harris, N. R. P., Bauguittie, S-J., Gallagher, M., Bacak, A., Leather, K. E.
10 and Percival, C. J.: Enhanced ozone loss by active inorganic bromine chemistry in the tropical troposphere, *Atmos.*
11 *Environ.*, 155, 21–28, 2017a.

12 Le Breton, M., Wang, Y., Hallquist, Å. M., Pathak, R. K., Zheng, J., Yang, Y., Shang, D., Glasius, M., Bannan,
13 T. J., Liu, Q., Chan, C. K., Percival, C. J., Zhu, W., Lou, S., Topping, D., Wang, Y., Yu, J., Lu, K., Guo, S., Hu,
14 M., and Hallquist, M.: Online gas and particle phase measurements of organosulfates, organosulfonates and
15 nitrooxyorganosulfates in Beijing utilizing a FIGAERO ToF-CIMS, *Atmos. Chem. Phys. Discuss.*,
16 <https://doi.org/10.5194/acp-2017-814>, in review, 2017b.

17 Liu, Y., Yuan, B., Li, X., Shao, M., Lu, S., Li, Y., Chang, C.-C., Wang, Z., Hu, W., Huang, X., He, L., Zeng, L.,
18 Hu, M., and Zhu, T.: Impact of pollution controls in Beijing on atmospheric oxygenated volatile organic
19 compounds (OVOCs) during the 2008 Olympic Games: observation and modeling implications, *Atmos. Chem.*
20 *Phys.*, 15, 3045–3062, <https://doi.org/10.5194/acp-15-3045-2015>, 2015.

21 Liu, J., D’Ambro, E. L., Lee, B. H., Lopez-Hilfiker, F., Zaveri, R. A., RiveraRios, J. C., Keutsch, F. N., Lyer, S.,
22 Kurtne, T., Zhang, Z., Gold, A., Surratt, J. D., Shilling, J. E. and Thornton, J. A.: Efficient Isoprene Secondary
23 Organic Aerosol Formation from a Non-IEPOX Pathway, *Environ. Sci. Technol.*, 50, 18, 9872–9880, 2016.

24 Lopez-Hilfiker, F. D., Mohr, C., Ehn, M., Rubach, F., Kleist, E., Wildt, J., Mentel, Th. F., Lutz, A., Hallquist, M.,
25 Worsnop, D., and Thornton, J. A.: A novel method for online analysis of gas and particle composition: description
26 and evaluation of a Filter Inlet for Gases and AEROSols (FIGAERO), *Atmos. Meas. Tech.* 2014, 7, 983–1001,
27 doi:10.5194/amt-7-983-2014.

28 Ma, Q., Shuxiao, S. C., Zhao, B., Martin, R. V., Brauer, M., Cohen, A., Jiang, J., Zhou, W., Hao, J., Frostad, J.,
29 Forouzanfar, M. H. and Burnett, T.: Impacts of coal burning on ambient PM1 pollution in China, *Atmos. Chem.*
30 *Phys.*, 17, 4477–4491, 2017.

31 Manion, J. A., R. E. Huie, R. D. Levin, D. R. Burgess Jr, V. L Orkin, W. Tsang, W. S. McGivern, J. W. Hudgens,
32 V. D. Knyazev, D. B Atkinson, E. Chai, A. M. Tereza, C.-Y. Lin, T. C. Allison, W. G. Mallard, F. Westley, J.
33 T. Herron, R. F. Hampson, and D. H. Frizzell (2014) NIST Chemical Kinetics Database, NIST Standard Reference
34 Database 17, Version 7.0 (Web Version), Release 1.6.8, Data version 2013.03, National Institute of Standards and
35 Technology, Gaithersburg, Maryland, 20899-8320. Web address: <http://kinetics.nist.gov/>

36 Mielke, L. H., Furgeson, A., Odam-Ankrah, C. A., and Osthoff, H. D.: Ubiquity of ClNO₂ in the urban boundary
37 layer of Calgary, AB, Canada, *Canadian J. Chem.*, 2015.

38 Nordmeyer, T., Wang, W., Ragains, M. L., Finlayson-Pitts, B. J., Spicer, C. W. and Plastridge, R. A.: Unique
39 products of the reaction of isoprene with atomic chlorine: Potential markers of chlorine atom chemistry, *Geophys.*
40 *Res. Lett.*, 24(13), 1615–1618, doi:10.1029/97GL01547, 1997.

41 Ofner, J., Balzer, N., Buxmann, J., Grothe, H., Schmitt-Kopplin, P., Platt, U. and Zetzsch, C.: Halogenation
42 processes of secondary organic aerosol and implications on halogen release mechanisms, *Atmos. Chem. Phys.*,
43 12(13), 5787–5806, doi:10.5194/acp-12-5787-2012, 2012.

- 1 Orlando, J. J., Tyndall, G. S., Apel, E. C., Riemer, D., and Paulson, S. E.: Rate coefficients and mechanisms of the
2 reaction of Cl-atoms with a series of unsaturated hydrocarbons under atmospheric conditions, *Int. J. Chem. Kinet.*,
3 35, 334–353, 2003.
- 4 Osthoff, H.D.; Roberts, J.M.; Ravishankara, a. R.; Williams, E.J.; Lerner, B.M.; Sommariva, R.; Bates, T.S.;
5 Coffman, D.; Quinn, P.K.; Dibb, J.E.:High levels of nitryl chloride in the polluted subtropical marine boundary
6 layer. *Nat. Geosci.* 2008, 1, 324–328, 2008.
- 7 Platt, U., Allan, W., and Lowe, D.: Hemispheric average Cl atom mixing ratio from $^{13}\text{C}/^{12}\text{C}$ ratios in atmospheric
8 methane, *Atmos. Chem. Phys.*, 4, 2393–2399, 4, 2004.
- 9 Phillips, G. J., Tang, M. J., Thieser, J., Brickwedde, B., Schuster, G., Bohn, B., Lelieveld, J., and Crowley, J. N.:
10 Significant mixing ratios of nitryl chloride observed in rural continental Europe associated with the influence of
11 sea salt chlorine and anthropogenic emissions, *Geophys. Res. Lett.*, 39, L10811, 2016.
- 12 Phillips, G. J., Thieser, J., Tang, M., Sobanski, N., Schuster, G., Fachinger, J., Drewnick, F., Borrmann, S.,
13 Bingemer, H., Lelieveld, J. and Crowley, J. N.: Estimating N_2O_5 uptake coefficients using ambient measurements
14 of NO_3 , N_2O_5 , ClNO_2 and particle-phase nitrate, *Atmos. Chem. Phys.*, 16, 13231-13249, 2016.
- 15 Pszenny, A. A. P., Fischer, E. V., Russo, R. S., Sive, B. C., and Varner, R. K.: Estimates of Cl atom mixing ratios
16 and hydrocarbon kinetic reactivity in surface air at Appledore Island, Maine (USA), during International
17 Consortium for Atmospheric Research on Transport and Transformation/Chemistry of Halogens at the Isles of
18 Shoals, *J. Geop*
- 19 Riedel, T. P., Bertram, T. H., Crisp, T. A., Williams, E. J., Lerner, B. M., Vlasenko, A., Li, S. M., Gilman, J., de
20 Gouw, J., Bon, D. M., Wagner, N. L., Brown, S. S., and Thornton, J. A.: Nitryl chloride and molecular chlorine in
21 the coastal marine boundary layer, *Environ. Sci. Technol.*, 46, 10463–10470, 2012.
- 22 Riedel, T. P., Wolfe, G. M., Danas, K. T., Gilman, J. B., Kuster, W. C., Bon, D. M., Vlasenko, A., Li, S. M.,
23 Williams, E. J., Lerner, B. M., Veres, P. R., Robert, J. M., Holloway, J. S., Lefer, B., Brown, S.S. and Thornton,
24 J. A.: An MCM modeling study of nitryl chloride (ClNO_2) impacts on oxidation, ozone production and nitrogen
25 oxide partitioning in polluted continental outflow, *Atmos. Chem. Phys.*, 14, 3789-3800, 2014.
- 26 Riemer, D. D., Apel, E. C., Orlando, J. J., Tyndall, G. S., Brune, W. H., Williams, E. J., Lonneman, W. A. and
27 Neece, J. D.: Unique isoprene oxidation products demonstrate chlorine atom chemistry occurs in the Houston,
28 Texas urban area, *J. Atmos. Chem.*, 61(3), 227–242, 2008.
- 29 Riva, M., Healy, R. M., Flaud, P. M., Perraudin, E., Wenger, J. C. and Villenave, E.: Gas- and Particle-Phase
30 Products from the Chlorine-Initiated Oxidation of Polycyclic Aromatic Hydrocarbons, *J. Phys. Chem. A*, 119(45),
31 11170–11181, doi:10.1021/acs.jpca.5b04610, 2015.
- 32 Roberts, J. M., Osthoff, H. D., Brown, S. S., and Ravishankara, A. R.: N_2O_5 oxidizes chloride to Cl_2 in acidic
33 atmospheric aerosol, *Science*, 321, 1059–1059, doi:10.1126/science.1158777, 2008.
- 34 Sander, R.: Modeling atmospheric chemistry: Interactions between gas-phase species and liquid cloud/aerosol
35 particles, *Surv. Geophys.*, 20, 1–31, 1999.
- 36 Sarwar, G., Simon, H., Xing, J., and Mathur, R.: Importance of tropospheric ClNO_2 chemistry across the Northern
37 Hemisphere, *Geophys. Res. Lett.*, 41, 4050–4058, 2014.
- 38 Simpson, D., Benedictow, A., Berge, H., Bergström, R., Emberson, L. D., Fagerli, H., Flechard, C. R., Hayman,
39 G. D., Gauss, M., Jonson, J. E., Jenkin, M. E., Nyíri, A., Richter, C., Semeena, V. S., Tsyro, S., Tuovinen, J.-P.,
40 Valdebenito, Á., and Wind, P.: The EMEP MSC-W chemical transport model – technical description, *Atmos.*
41 *Chem. Phys.*, 12, 7825-7865, <https://doi.org/10.5194/acp-12-7825-2012>, 2012.

1 Simon, H., Y. Kimura, G. McGaughey, D.T. Allen, S.S. Brown, H.D. Osthoff, J.M. Roberts, 422 D. Byun, and D.
2 Lee.: Modeling the impact of ClNO₂ on ozone formation in the 423 Houston area, *J. Geophys. Res.*, 114, D00F03,
3 424 doi:10.1029/2008JD010732, 2009.

4 Skamarock, W. C., J. B. Klemp, J. Dudhia, D. O. Gill, D. M. Barker, M. G Duda, X.-Y. Huang, W. Wang, and J.
5 G. Powers, 2008: A Description of the Advanced Research WRF Version 3. NCAR-Tech, 113,
6 doi:10.5065/D68S4MVH

7 Tanaka, P. L., Riemer, D. D., Chang, S., Yarwood, G., McDonaldBuller, E. C., Apel, E. C., Orlando, J. J., Silva,
8 P. J., Jimenez, J. L., Canagaratna, M. R., Neece, J. D., Mullins, C. B., and Allen, D. T.: Direct evidence for
9 chlorine-enhanced urban ozone formation in Houston, Texas, *Atmos. Environ.*, 37, 1393–1400, 2003.

10 Tham, Y., Yan, C., Xue, L., Zha, Q., Wang, X., and Wang, T.: Presence of high nitryl chloride in Asian coastal
11 environment and its impact on atmospheric photochemistry, *China Sci. Bull.*, 59, 356–359, doi:10.1007/s11434-
12 013-0063-y, 2014.

13 Thornton, J. A., Kercher, J. P., Riedel, T. P., Wagner, N. L., Cozic, J., Holloway, J. S., Dube, W. P., Wolfe, G. M.,
14 Quinn, P. K., Middlebrook, A. M., Alexander, B., and Brown, S. S.: A large atomic chlorine source inferred from
15 mid-continental reactive nitrogen chemistry, *Nature*, 464, 271–274, doi:10.1038/nature08905, 2010.

16 Wagner, N. L., Riedel, T. P., Young, C. J., Bahreini, R., Brock, C. A., Dube, W. P., Kim, S., Middlebrook, A. M.,
17 Öztürk, F., Robert, J. M., Russo, R., Sive, B., Swarthout, R., Thornton, J. A., VandenBoer, T. C., Zhou, Y. and
18 Brown, S. S.: N₂O₅ uptake coefficients and nocturnal NO₂ removal rates determined from ambient wintertime
19 measurements, 118, 16, 9331-9350, 2013.

20 Wang, W. and Finlayson-Pits, B. J.: Unique markers of chlorine atom chemistry in coastal urban areas: The
21 reaction with 1,3-butadiene in air at room temperature, *J. Geophys. Res.*, 106, 5, 4939-4958, 2001.

22 Wang, T., Cheung, T., Li, Y., Yu, X. and Blake, D.: Emission characteristics of CO, NO_x, SO₂ and indications of
23 biomass burning observed at a rural site in eastern China. *J. Geophys. Res. Atmos.*, 107, 12, 2002.

24 Wang, T., Tham, Y.J., Xue, L., Li, Q., Zha, Q., Wang, Z., Poon, S.C.N., Dube, W.P., Blake, D.R., Louie, P.K.K.,
25 Luk, C.W.Y., Tsui, W., Brown, S.S.: Observations of nitryl chloride and modeling its source and effect on ozone
26 in the planetary boundary layer of southern China. *J. Geophys. Res.* 121, 2476e2489, 2016

27 Wang, H., Chen, J. and Lu, K.: Development of a portable cavity-enhanced absorption spectrometer for the
28 measurement of ambient NO₃ and N₂O₅: experimental setup, lab characterizations, and field applications in a
29 polluted urban environment, *Atmos. Chem. Phys.*, 10, 1465-1479, 2017.

30 Wang, X., Wang, H., Xue, L., Wang, T., Wang, L., Gu, R., Wang, W., Than, Y. T., Wang, Z., Yang, L., Chen, J.
31 and Wang, W.: Observations of N₂O₅ and ClNO₂ at a polluted urban surface site in North China: High N₂O₅ uptake
32 coefficients and low ClNO₂ product yields, *Atmos. Environ.*, 156, 125-134, 2017.

33 Wang, Z., Wang, W., Tham, Y. J., Hao, Q. L., Wang, L. W., Xinfeng., W., Wang, L. W. and Wang, T.: Fast
34 heterogeneous N₂O₅ uptake and ClNO₂ production in power plant plumes observed in the nocturnal residual layer
35 over the North China Plain, *Atmos. Chem. Phys. Discuss.*, 2017.

36 Wang, D. and Ruiz, L. H.: Secondary organic aerosol from chlorine-initiated oxidation of isoprene, *Atmos. Chem.*
37 *Phys. Discuss.*, 2017-342, 2017.

38 Whalley, L. K., Furneaux, K. L., Goddard, A., Lee, J. D., Mahajan, A., Oetjen, H., Read, K. A., Kaaden, N.,
39 Carpenter, L. J., Lewis, A. C., Plane, J. M. C., Saltzman, E. S., Wiedensohler, A., and Heard, D. E.: The chemistry
40 of OH and HO₂ radicals in the boundary layer over the tropical Atlantic Ocean, *Atmos. Chem. Phys.*, 10, 1555-
41 1576, <https://doi.org/10.5194/acp-10-1555-2010>, 2010.

1 Wiedinmyer, C., S. K. Akagi, R. J. Yokelson, L. K. Emmons, J. A. Al-Saadi, J. J. Orlando, and A. J. Soja. "The
2 Fire Inventory from Ncar (Finn): A High Resolution Global Model to Estimate the Emissions from Open Burning."
3 Geoscientific Model Development 4, no. 3 (2011): 625-41.

4 Ye, Y., Galbally, I. E., Weeks, I. A., Duffy, B. L., and Nelson, P. F.: Evaporative emissions of 1,3-butadiene from
5 petrol-fuelled motor vehicles, Atmos. Environ., 32, 2685–2692, 1998.

6 Young, C. J., Washenfelder, R. A., Roberts, J. M., Mielke, L. H., Osthoff, H. D., Tsai, C., Pikelnaya, O., Stutz, J.,
7 Veres, P. R., Cochran, A. K., VandenBoer, T. C., Flynn, J., Grossberg, N., Haman, C. L., Lefer, B., Stark, H.,
8 Graus, M., de Gouw, J., Gilman, J. B., Kuster, W. C., and Brown, S. S.: Vertically Resolved Measurements of
9 Nighttime Radical Reservoirs; in Los Angeles and Their Contribution to the Urban Radical Budget, Environ. Sci.
10 Technol., 46, 10965–10973, doi:10.1021/es302206a, 2012.

11 Zou, Q., Lu, K. D., Wu, Y. S., Yang, Y. D., Du, Z. F., and Hu, M.: Ambient photolysis frequency of NO₂ determ
12 ined using chemical actinometer and spectroradiometer at an urban site in Beijing, Front Env Sci Eng, 10, ARTN
13 13 10.1007/s11783-016-0885-3, 2016.

14

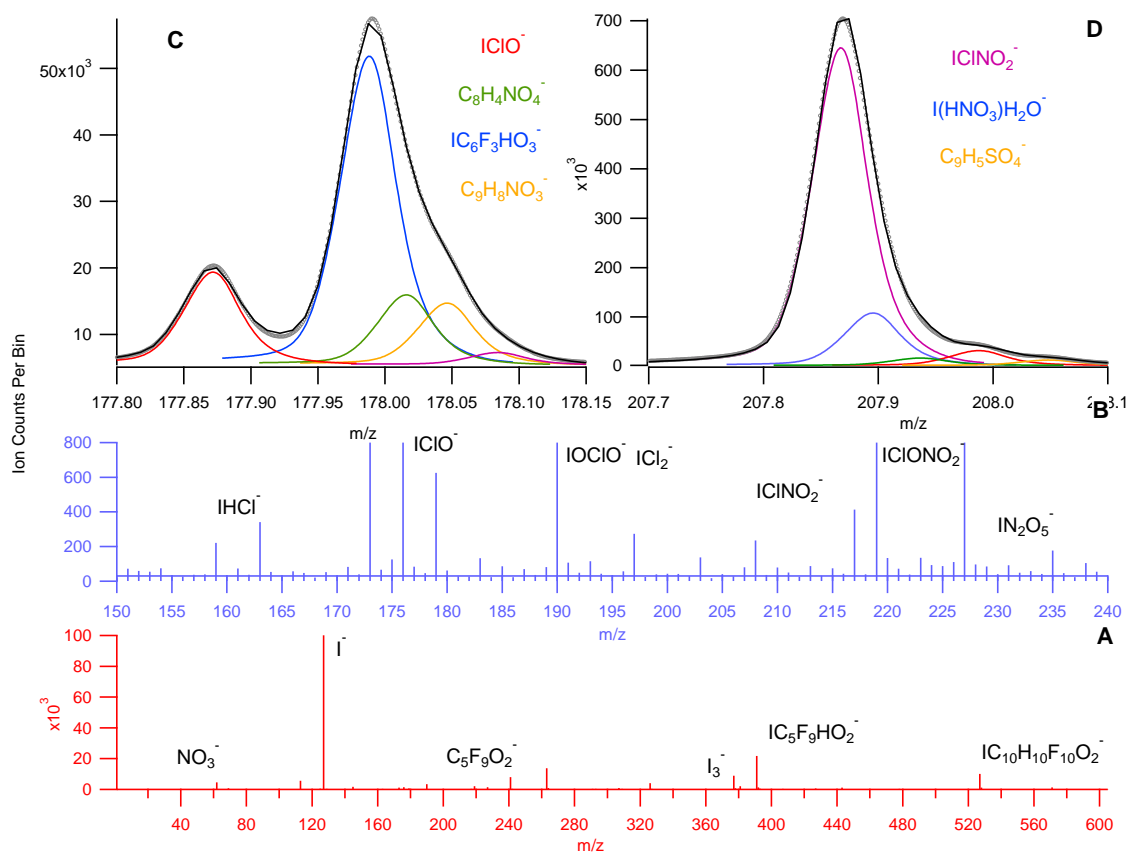
15 **Table 1. Identified Cl-VOC reaction products, nomenclature of Cl-VOC and precursor compound.**

Cl-VOC	Potential nomenclature	Precursor
CHClO	formyl chloride	formaldehyde
C ₂ H ₃ ClO	chloroacetaldehyde	acetaldehyde
C ₃ H ₅ ClNO ₅	Chloro PPN	PPN
C ₂ H ₃ ClNO ₅	chloro PAN	PAN
C ₃ H ₅ ClO	chloroacetone	acetone
C ₂ H ₃ ClO ₂	chloroacetic acid	acetic acid
CHClO ₂	chloroformic acid	formic acid
C ₄ H ₇ ClO	chloro MEK or butanal	isoprene
C ₅ H ₆ ClO	CMBO - chloro 3-methyl-3-butene-2-one	isoprene
C ₅ H ₉ ClO ₂	-	isoprene
C ₅ H ₉ ClO ₃	-	isoprene
C ₃ H ₅ ClO	propanoyl chloride	1, 3 butadiene
C ₈ H ₉ Cl	chloroethyl benzene	aromatic

16

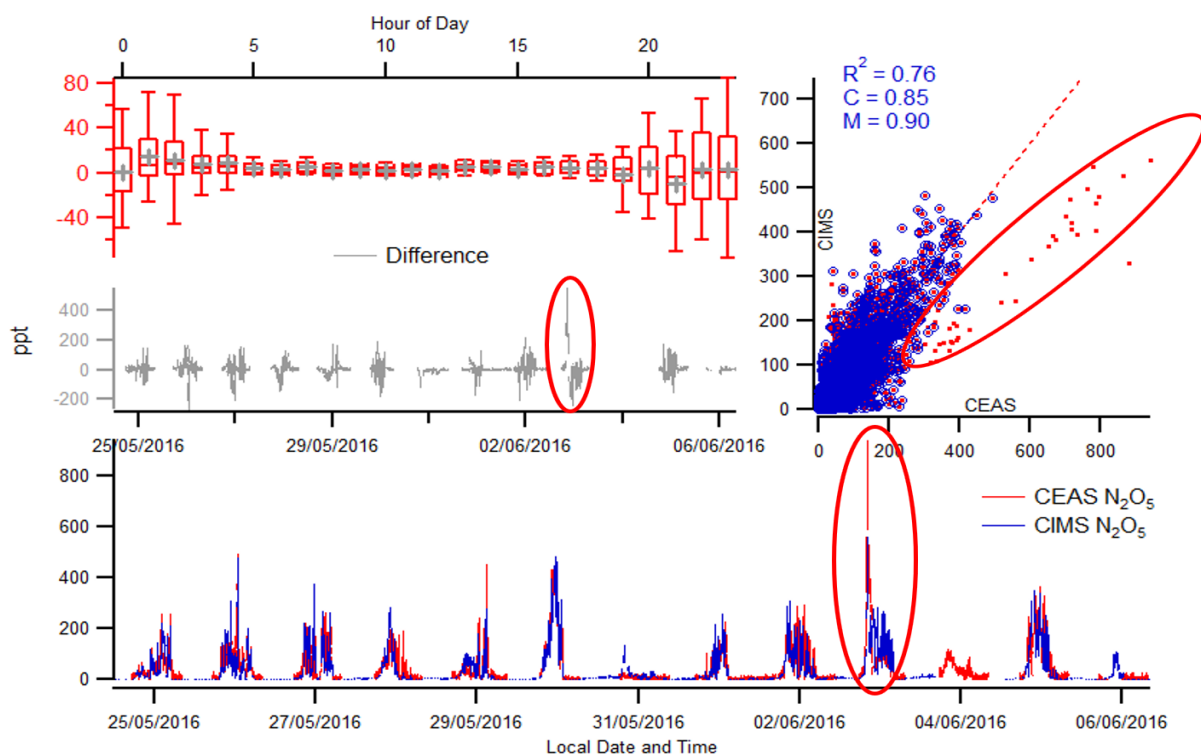
17

1



2

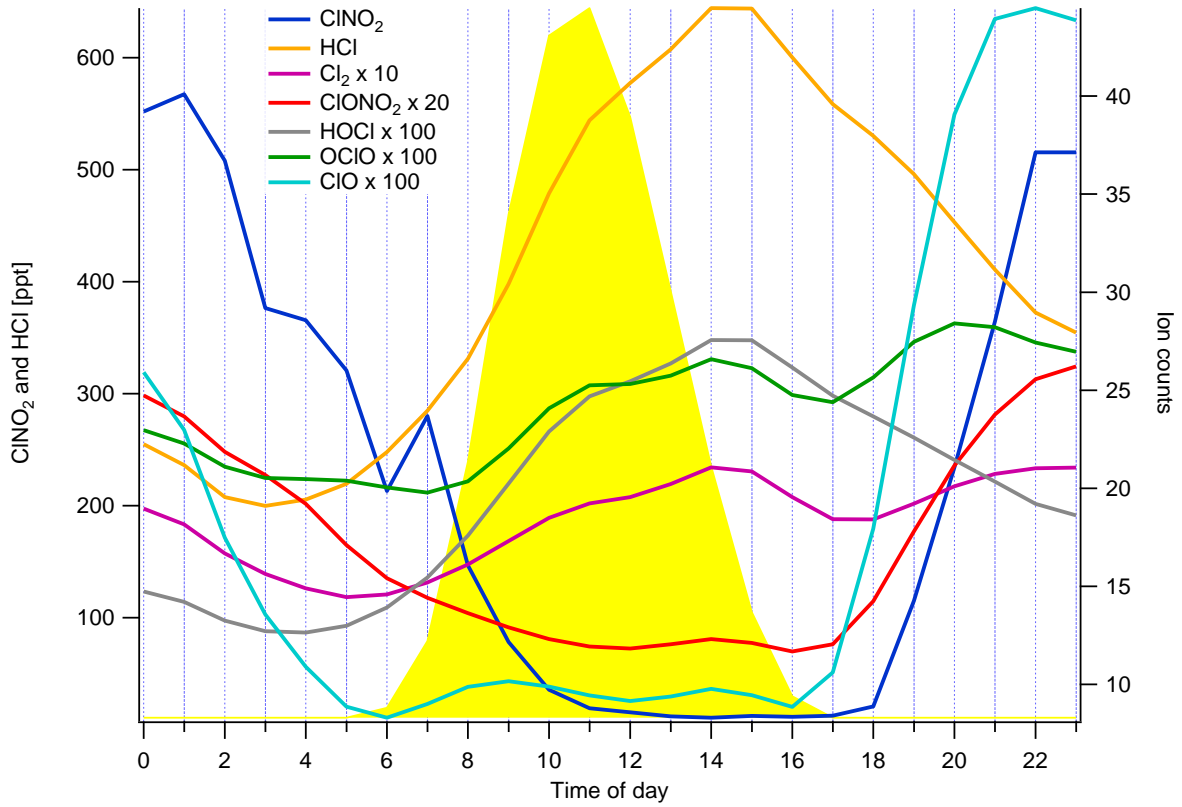
3 **Figure 1. Panel A: Average mass spectrum for the whole measured range. Panel B: Average mass spectrum**
 4 **for the region that contains all gas phase night time species utilised in this work. A high resolution spectral**
 5 **fit for ClO and ClNO₂ are displayed with corresponding multi peaks with 0.5 AMU (panels C and D). The**
 6 **black line represents the total fit from all peaks. The grey line represents the mass spectral raw data.**



1

2 **Figure 2. CIMS and CEAS one minute averaged data of N_2O_5 with corresponding correlation plot (panel**
 3 **A), campaign and diurnal deviation (panels B and C respectively). The red highlighted periods represent**
 4 **data collected on the 3rd June where a different correlation gradient was observed between CIMS and**
 5 **CEAS. The box and whisker plot represents the diurnal difference for the campaign between the CEAS and**
 6 **CIMS measurements (panel D). C is the y-intercept of the line of best fit and M is the gradient.**

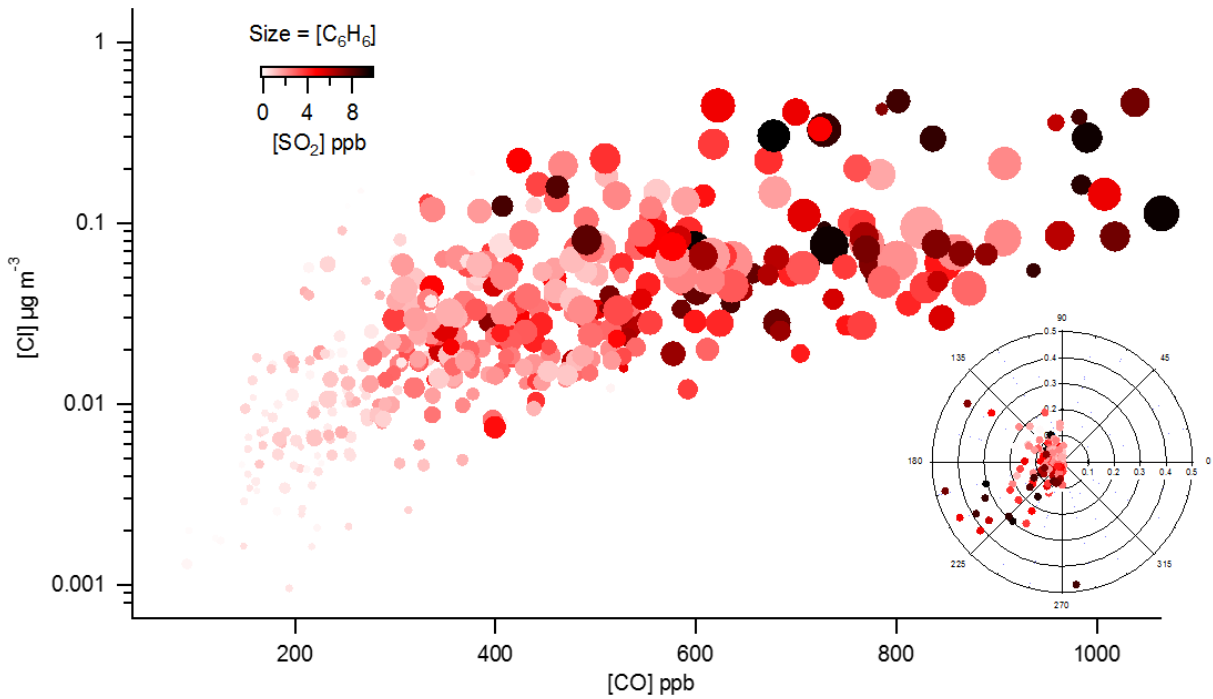
7



1

2 **Figure 3. Mean diurnal profiles of the inorganic halogens detected by the CIMS from the 23rd May to 6th**
 3 **June with average J rate for ClNO₂ as guide for photolysis. ClNO₂ and HCl mixing ratios are on the left y-**
 4 **axis and the other inorganic halogens on the right y-axis displayed in ion counts.**

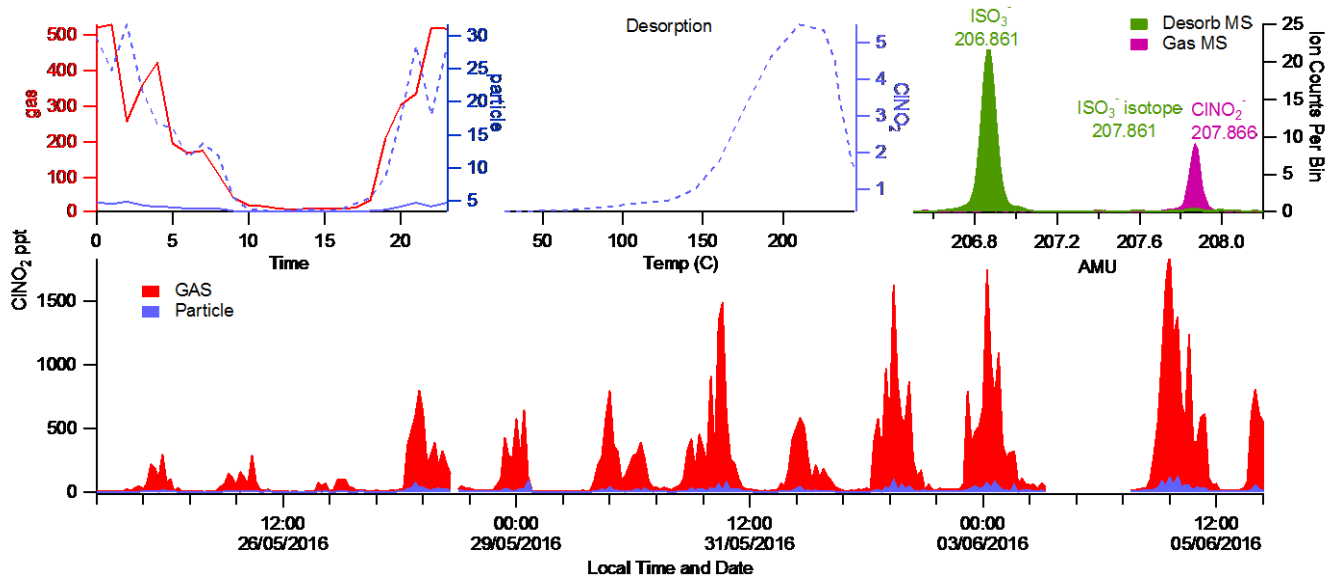
5



6

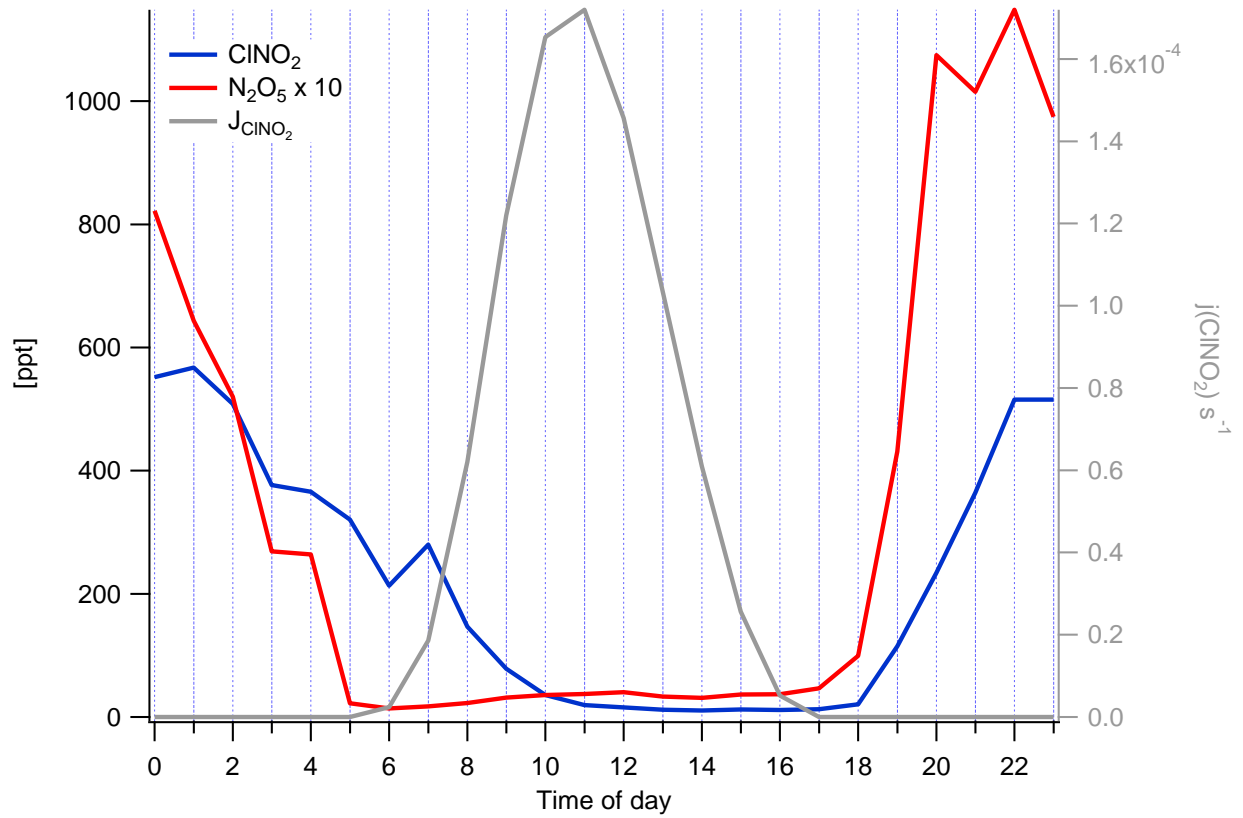
1 Figure 4. Correlation of particulate Cl⁻ from the AMS measurements and CO colour coded by SO₂ mixing
 2 ratio and size binned by increasing benzene mixing ratio. A wind rose plot illustrates the wind direction and
 3 particulate Cl⁻ mixing ratio colour coded by SO₂ mixing ratio.

4
 5
 6



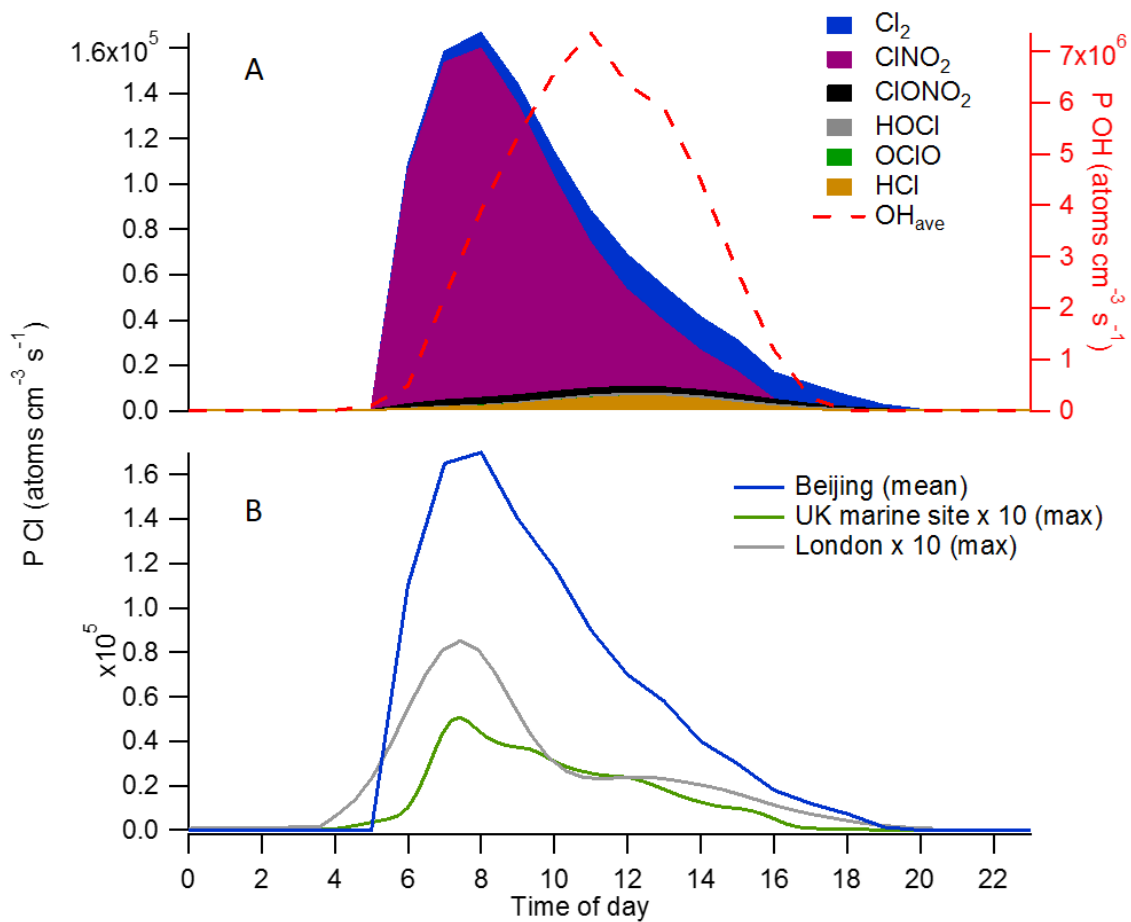
7
 8 Figure 5. CINO₂ gas and particle phase campaign time series (1 hour averaged) (panel A) and average
 9 diurnal profiles Panel B). The peak fitting for CINO₂ and the SO₃ interfering mass at 207-208 AMU (panel
 10 C) and the desorption profile for the counts attributed to the high resolution CINO₂ peak (panel D).

11



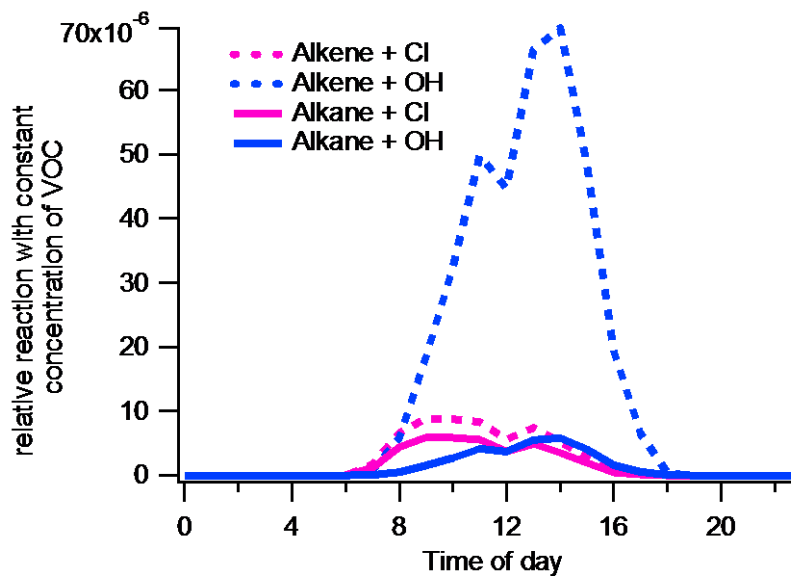
1

2 **Figure 6. Diurnal profile of N₂O₅, ClNO₂ and j(ClNO₂) for the campaign highlighting the persistence of**
 3 **ClNO₂ passed sunrise and the expected rapid photolysis of N₂O₅.**



1

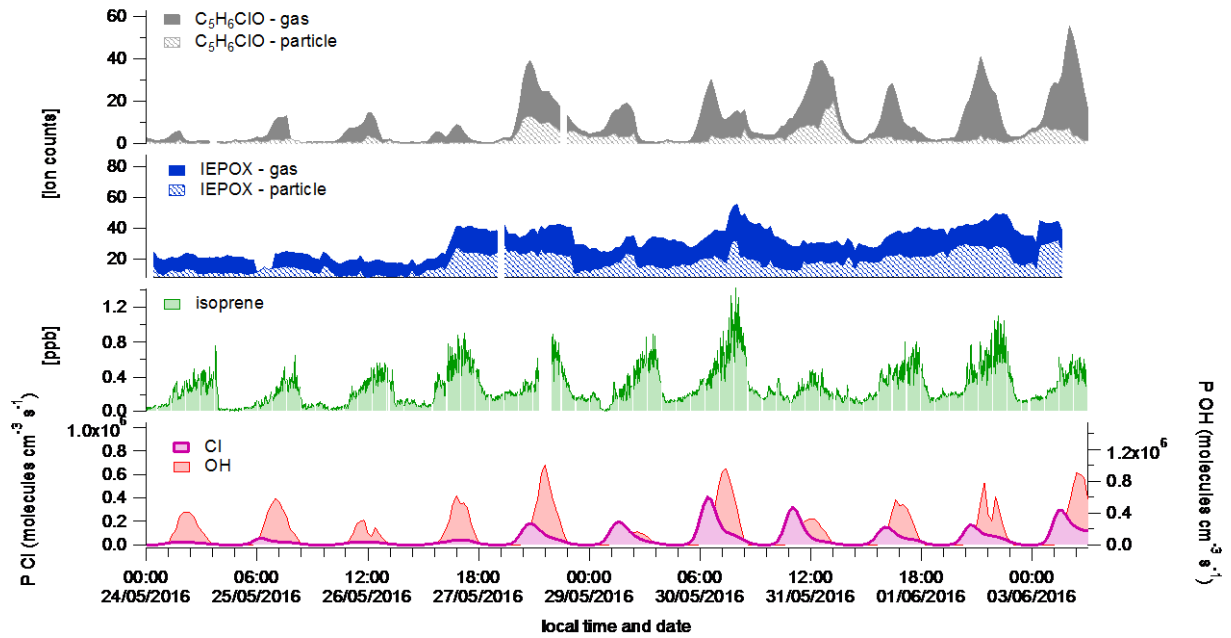
2 **Figure 7. A) Steady state calculation of inorganic halogens contribution to chlorine atom production. B)**
 3 **Relative mean diurnal profiles of calculated chlorine atom mixing ratio calculation from this work (Beijing)**
 4 **and measurements in the UK (London (Bannan et al., 2015) and a marine site (Weybourne Atmospheric**
 5 **Observatory-Bannan et al., (2017)). The steady state OH production rate from Beijing is also displayed to**
 6 **illustrate relative mixing ratios of oxidants.**



7

1 **Figure 8. Mean diurnal time series of alkene (pink) and alkane (blue) relative reaction rate (arbitrary value)**
 2 **with the chlorine atom (dashed) and OH (solid).**

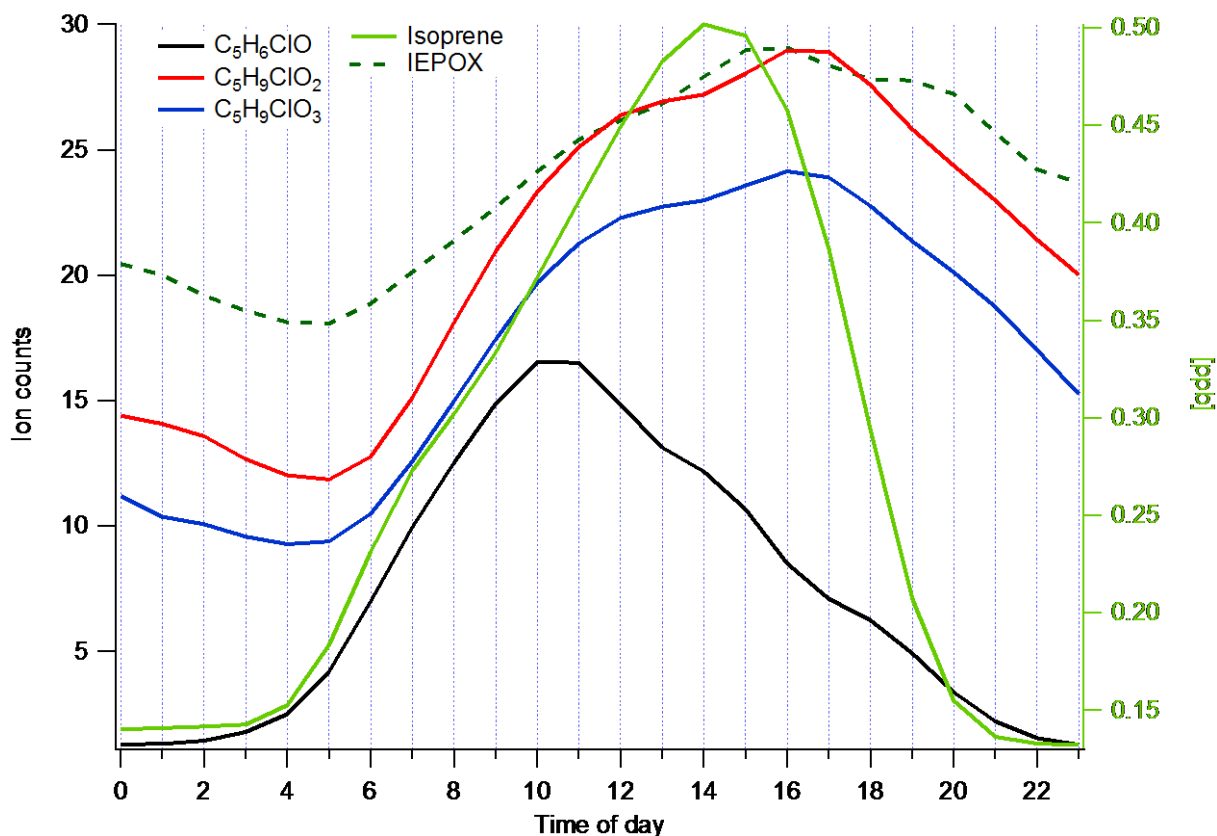
3



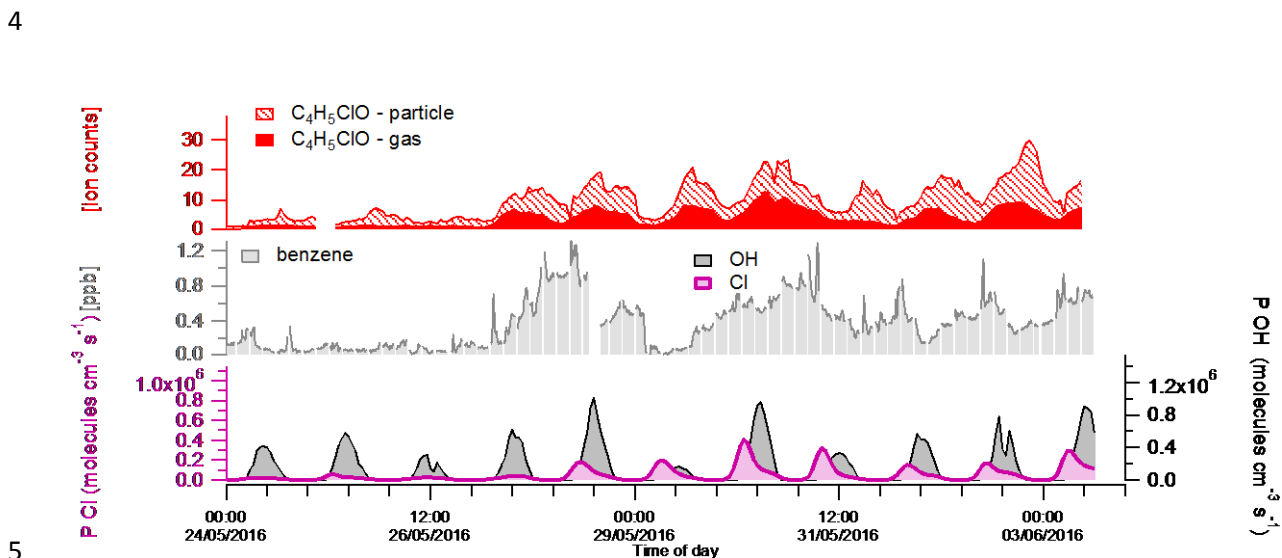
4

5 **Figure 9. Campaign time series of isoprene, IEPOX, CMBO and steady state production rate of chlorine**
 6 **atoms and OH**

7

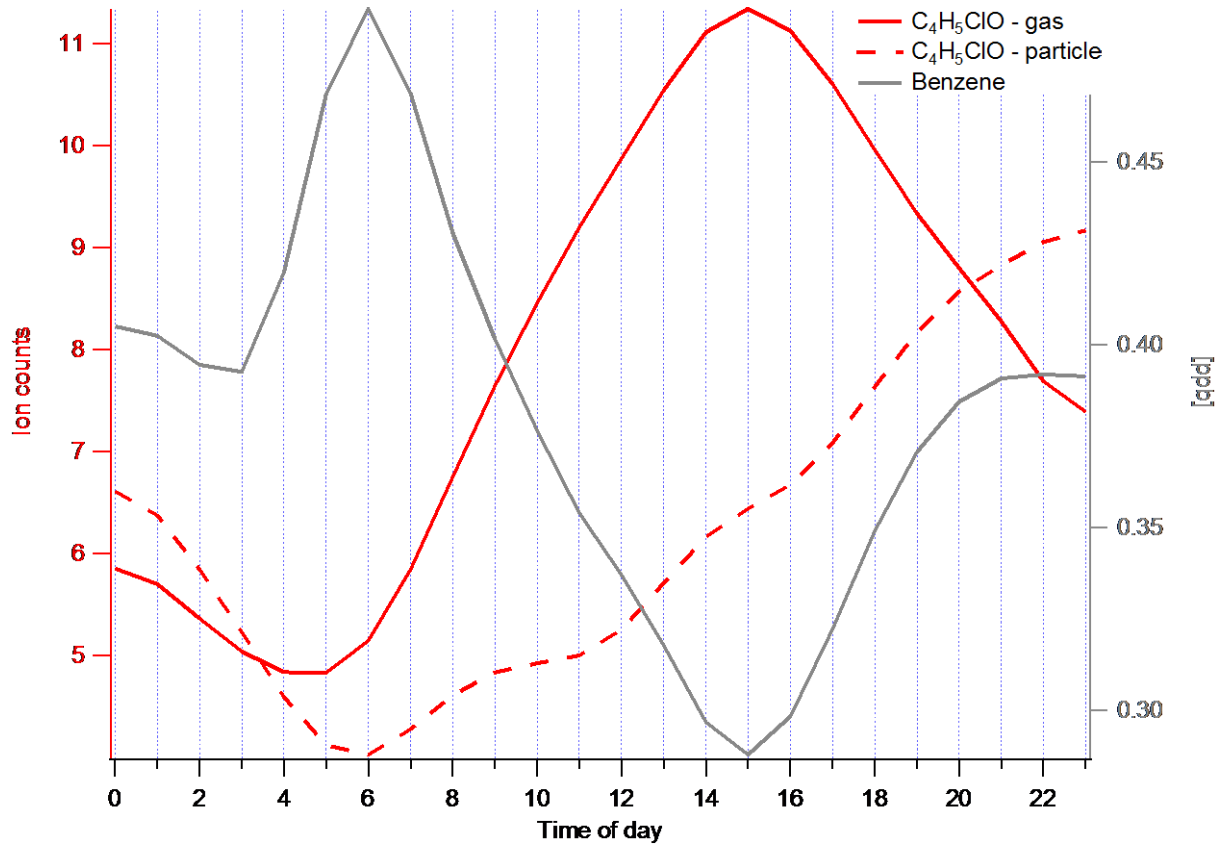


1
 2 **Figure 10. Mean diurnal profiles of isoprene (right y-axis) and its OH oxidation product (IEPOX) and**
 3 **chlorine atom oxidation products CMBO, $C_5H_9ClO_2$ and $C_5H_9ClO_3$ (left y-axis)**



5
 6 **Figure 11. Campaign time series of benzene and CCA with supporting calculations of OH and the chlorine**
 7 **atom production rates**

8



1

2 **Figure 12. Mean campaign diurnal profiles of benzene (grey) and CCA in the particle (dashed red) and gas**
 3 **phase (solid red).**

4